Theoretical study of the electronic states of Nb 4 , Nb 5 clusters and their anions (Nb 4 − , Nb 5 −)

D. Majumdar and K. Balasubramanian

Citation: The Journal of Chemical Physics **121**, 4014 (2004); doi: 10.1063/1.1769358
View online: http://dx.doi.org/10.1063/1.1769358
View Table of Contents: http://scitation.aip.org/content/aip/journal/jcp/121/9?ver=pdfcov
Published by the AIP Publishing

Theoretical study of the electronic states of Nb_4, Nb_5 clusters and their anions (Nb_4^-,Nb_5^-)

D. Majumdar
Center for Image Processing and Integrated Computing, University of California Davis, Livermore, California 94550

K. Balasubramanian[a)]
Center for Image Processing and Integrated Computing, University of California Davis, Livermore, California 94550; Chemistry & Material Science Directorate, Lawrence Livermore National Laboratory, University of California, Livermore, California 94550; and Glenn T. Seaborg Center, Lawrence Berkeley National Laboratory, Berkeley, California 94720

(Received 19 March 2004; accepted 17 May 2004)

Geometries and energy separations of the various low-lying electronic states of Nb_n and Nb_n^- ($n=4,5$) clusters with various structural arrangements have been investigated. The complete active space multiconfiguration self-consistent field method followed by multireference singles and doubles configuration interaction (MRSDCI) calculations that included up to 52×10^6 configuration spin functions have been used to compute several electronic states of these clusters. The ground states of both Nb_4 ($^1A'$, pyramidal) and Nb_4^- ($^2B_{3g}$, rhombus) are low-spin states at the MRSDCI level. The ground state of Nb_5 cluster is a doublet with a distorted trigonal bipyramid (DTB) structure. The anionic cluster of Nb_5 has two competitive ground states with singlet and triplet multiplicities (DTB). The low-lying electronic states of these clusters have been found to be distorted due to Jahn-Teller effect. On the basis of the energy separations of our computed electronic states of Nb_4 and Nb_5, we have assigned the observed photoelectron spectrum of Nb_n^- ($n=4,5$) clusters. We have also compared our MRSDCI results with density functional calculations. The electron affinity, ionization potential, dissociation and atomization energies of Nb_4 and Nb_5 have been calculated and the results have been found to be in excellent agreement with the experiment.
 [DOI: 10.1063/1.1769358]

I. INTRODUCTION

The advent of gas-phase experimental methods of small transition metal clusters has opened up a new and exciting research area that affords the opportunity to study the electronic states and changes in metal chemistry as a function of size. The low-lying electronic states of transition metal clusters pose considerable challenge to the quantum chemists due to large electron correlation effects and the existence of several low-lying electronic states of different spatial symmetries and spin multiplicities. Small niobium clusters are among the most thoroughly studied transition metal clusters by experiment. Extensive gas-phase investigations have been carried out on these clusters concerning their chemical reactivity, photoelectron spectroscopy, and physical properties that include ionization potentials (IPs), electron affinities (EAs), and atomization energies (AEs).[1–6] Theoretical studies of these clusters cannot only provide interpretation of such experimental results but also facilitate a tractable platform to understand the metal-metal bonding and reactivity of small molecules on the metal surface. Due to complex nature of electron correlation effects, the relative order of the electronic states and their structural properties change significantly as a function of theoretical treatment. Furthermore, the results of computational studies on small metal clusters provide a link between the molecular and solid states.

Niobium clusters of various sizes have been produced by pulsed laser vaporization of compressed niobium powder[1,7,8] and a series of experiments on the reactivity of niobium clusters have been conducted using fast flow reactor techniques,[9–11] flow tube,[12] and guided ion beam measurements.[5] Armentrout and co-workers[5,6] have measured the stepwise dissociation energies of Nb_n ($n=2-6$) and Nb_n^+ ($n=2-11$) clusters using a collision induced dissociation (CID) technique. They have found that the dissociation energies (D_e) of Nb_n do not change monotonically with respect to the cluster size. The D_e value of Nb_3 is the lowest among these clusters ($n=2-6$) and Nb_4 is the most stable one ($D_e=5.9$ eV). The D_e values of all these clusters are larger than 4.0 eV, indicating that these clusters are strongly bound. The D_e values of Nb_n^+ clusters[5] also follow the same trend.

The Nb_n clusters are quite reactive analogous to their cationic counterparts. Berces and co-workers[2] have studied the reaction of Nb_n clusters with nitrogen and deuterium using a flow tube reactor with a laser vaporization cluster source and time of flight mass spectrometer detector. Recently, Pederson and co-workers[13] have observed through their photoionization studies that the CO molecule adsorbs dissociatively on the Nb_3 surface. The niobium carbides,

a)Author to whom correspondence should be addressed; FAX: 925-422-6810. Electronic mail: kbala@ucdavis.edu

Nb_nC_m, have been the topic of extensive theoretical and experimental research.[14–16]

Earlier theoretical studies of small niobium clusters (neutral and anionic) have been focused mainly at the density functional (DFT) level. Fowler, Garcia, and Ugalde[17] have studied the neutral Nb_3 and Nb_4 clusters at the DFT level. They have predicted that the equilibrium ground state structures of Nb_3 and Nb_4 clusters are isosceles triangle ($^2B_1, C_{2v}$) and tetrahedral ($^1A_1, T_d$), respectively. Earlier density functional studies by Salahub and co-workers[18] on $Nb_n\,(n=2-7)$ have also confirmed similar structures for Nb_3 and Nb_4 clusters. They have further observed that the neutral clusters, in their ground states, always tried to remain in their lowest possible spin state. More recent DFT studies by Grönbeck and co-workers[19] on the neutral and ionic $Nb_n\,(n=8-10)$ clusters have indicated that the ground states of the larger clusters are always in their lowest possible spin states. The ground states of these clusters are competitive in nature, as the various isomers of these clusters are very close in energy.[19] Such closely spaced energy spectrum sometimes changes the behavior of such metal clusters. This was observed both theoretically and experimentally in the IP values of the Nb_9 cluster.[19]

Kietzmann and co-workers[3] have studied the photoelectron spectra (PES) of small niobium cluster anions $[Nb_n^-\,(n=3-8)]$ using a laser vaporization technique. The authors have inferred by comparison of experiment with their local spin density (LSD) calculations that the Nb_n^- clusters are in their lowest possible spin states. They have also inferred that although for Nb_3^- and Nb_5^- the singlet states (D_{3h} symmetry) are the lowest in energies, the triplet states (in C_{2v} and C_s symmetries for the trimer and pentamer, respectively) were more suitable candidates to interpret the experimental data. Fournier, Pang, and Chen[20] have carried out LSD calculations on the anionic clusters to assign the ground and excited states of the neutral Nb_n clusters from the observed PES. They have used a scaling technique on the calculated virtual orbital energies to assign the excited states of the neutral clusters. The technique was used to locate the excited states in the spectra, although such studies need to be validated at higher levels since electron correlation effects appear to change the relative orderings of these states. Moreover, all of the techniques that have been used up to now are based on single reference wave functions, while we consider multireference treatments.

It is well known that the wave functions are usually multireference in character for small transition metal clusters, and consequently, there could be several low-lying electronic states close to the ground state, making the spectra of these clusters extremely complicated. In our previous paper,[21] we have carried out a detailed high-level *ab initio* calculations on the Nb_3 and Nb_3^- at the *complete active space multiconfiguration self-consistent field* (CASMCSCF) and *multirefence singles and doubles configuration interaction* (MRSDCI) levels. It was evident from our studies that these clusters, like their cationic analogs, are multireference in character in their ground and low-lying electronic states, and most of these low-lying electronic structures undergo Jahn-Teller distortion. The last feature is not best revealed at the previous single reference level of theories. Apart from Nb_3 and Nb_3^-, there is no information on the nature of the excited electronic states of $Nb_n\,(n\geqslant 4)$ at the multireference level of theory. Such theoretical investigations, on the other hand, are crucial to interpret the observed electronic properties of the $Nb_n\,(n\geqslant 4)$ clusters.

The present paper deals with the structural and electronic properties of Nb_4, Nb_5, and their anionic clusters. These clusters are not only important due to their complicated PES, but also because of their structural distortion in various electronic states due to the Jahn-Teller effect.[22–24] First we report here the results of electronic structure calculations and the energy separations of the various low-lying electronic states of these clusters. We have used our energy separations to assign five observed peaks in the PES of Nb_4^-, and Nb_3^-.

Our previous studies on the niobium trimer have indicated that the low-lying electronic states of this cluster have Jahn-Teller distorted triangular (C_{2v}) geometries. That is, if a D_{3h} structure of the electronic state belongs to E' or E'' representation, it would be distorted due to the $E\otimes e$ Jahn-Teller coupling.[23,24] It could be seen from our present energy calculations that most of the low-lying electronic states of Nb_4 and Nb_5 undergo Jahn-Teller distortion. The calculation of IP, EA, dissociation energy (D_e), and the AE of the Nb_4 and Nb_5 are then presented together with a comparison of these results with experiment. Finally, a detailed analysis on the orbital and the charge distribution characteristics of different low-lying electronic states of Nb_4, Nb_5 and their anions are made.

II. METHODS OF COMPUTATION

The computations have been carried out using CASMCSCF followed by MRSDCI computations on the various electronic states of these metal clusters. Full geometry optimizations were carried out for each of the electronic states of these metal clusters at the CASMCSCF level using a quasi-Newton-Raphson[25] technique. The geometries of these clusters were also optimized at the DFT level of theory[26] to seek insight into their stable geometries at different spin multiplicities. However, the results must be considered cautiously since the electronic states of these clusters are multireference in character. The DFT calculations have used Becke's three parameter functional[27] with local correlation part provided by Vosko *et al.*[28] and the nonlocal part by Lee, Yang, and Parr[29] (in short, B3LYP). This DFT/B3LYP technique has been further used to compute the vibrational frequencies of the low-lying electronic states of these clusters.

The various possible geometries of Nb_4 and Nb_5 that we have considered here are shown in Fig. 1. Tetragonal (rhombus and square) and pyramidal (tetrahedral and distorted tetrahedral) geometries were considered to be the starting points for Nb_4. The calculations for the pyramidal structures were carried out in the C_s group, whereas the tetragonal structures were considered in the C_{2v} group. The tetragonal and the pyramidal structures can have special bent structural arrangements in the C_{2v} and D_2 groups. These structural arrangements were considered in the DFT/B3LYP calculations to compare with the previous DFT results of Fowler,

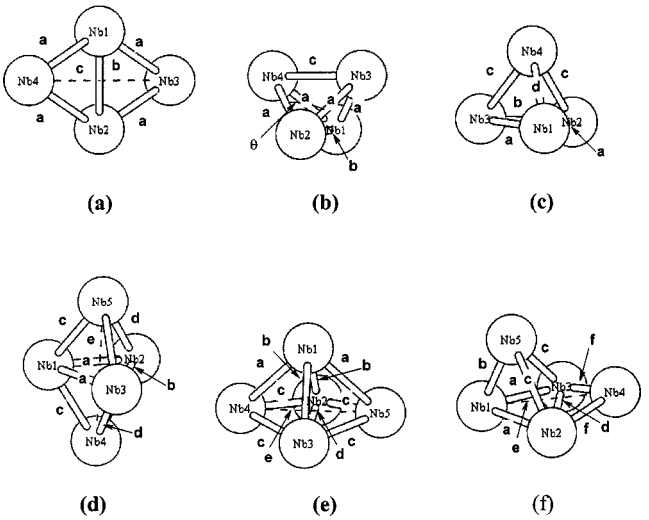

FIG. 1. Optimized structures of Nb_4 and Nb_5 clusters. The structures *a*, *b*, and *c* are the rhombus (D_{2h},^1A_g), D_2 (^5A), and pyramidal (C_s,$^1A'$) structures of Nb_4, while *d*, *e*, and *f* are the distorted trigonal bipyramid (C_{2v},$^2A_2$), distorted tetragonal pyramid (C_{2v},$^4A_1$), and distorted edge-capped tetrahedron (C_s,$^2A''$) structures of Nb_5. The optimized $D_2(b)$ structure is at the DFT/B3LYP level, while the other optimized structures are at the CASMCSCF level. The optimized values of the structural parameters (marked as *a*, *b*, *c*, *d*,...) for the various electronic states of Nb_n, and Nb_n^- ($n=4,5$) clusters are available in Tables I–IV (Nb_n) and VI–IX (Nb_n^-).

Garcia, and Ugalde.[17] The various geometries considered for the Nb_5 cluster include a regular trigonal bipyramid (D_{3h}), a distorted trigonal bipyramid (C_{2v}), a tetragonal pyramid (C_{4v}), a distorted tetragonal pyramid (C_{2v}), an edge-capped tetrahedron (C_{2v}), and a distorted edge-capped tetrahedron (C_s). The calculations for the edge-capped tetrahedron were carried out in the C_s group, whereas the calculations for all other clusters were made in the C_{2v} group. Relativistic effective core potentials (RECP) that replaced all but the outer $4s^24p^64d^45s^1$ shells by core potentials[30] were used in the present study. The corresponding optimized Gaussian basis set $(5s5p4d)$ was contracted to $(5s3p2d)$, with three large coefficients of *p* and *d* functions contracted. This choice of basis set is based on our previous study on the Nb_n^+ ($n=3-5$),[31] Nb_3, and Nb_3^- clusters.[21] However, the calculation of EA needs extended basis sets. We have carried out the EA calculation by augmenting the basis sets with $4f$ ($\zeta=0.45$) functions (at the CASMCSCF, MRSDCI, and DFT/B3LYP levels) and $5g$ ($\zeta=0.5505$) functions (at the DFT/B3LYP level). These *f* and *g* function's ζ values are optimized for energy. We have also included diffuse *s* ($\zeta=0.0148$), *p* ($\zeta=0.0081$), and *d* ($\zeta=0.035$) functions in the basis set at the DFT/B3LYP level. Thus the final basis sets for the EA calculations, at this level, are $(6s6p5d1f//6s4p4d1f)$ and $(6s6p5d1f1g//6s4p4d1f1g)$ including *f* and *g* functions, respectively. It is to be mentioned in this connection that although all-electron basis sets are desirable for the *ab initio* calculations, it is not practical to use such basis sets for heavy transition metal clusters. The effective core potential approach offers an alternate way to carry out such calculations by keeping the important valence space electrons of the atoms for explicit treatment. Moreover, the RECPs include relativistic effects such as mass-velocity and Darwin effects in a convenient manner.

The full active space of Nb_4 and Nb_4^- includes 40 orbitals and they correlate into $14a_1$, $10b_2$, $10b_1$, and $6a_2$ orbitals in the C_{2v} structure and $24a'$ and $16a''$ orbitals in the C_s structure. Likewise, the full active space of Nb_5 and Nb_5^- includes 50 orbitals correlating into $19a_1$, $12b_2$, $12b_1$, and $7a_2$ orbitals of the structures considered in the C_{2v} group, and $31a'$ and $19a''$ orbitals of the structures considered in the C_s symmetry. Inclusion of all these orbitals in the active space at the CASMCSCF level leads to too large a number of configuration spin functions (CSFs). To make the computations tractable, we have considered an alternative restricted active space approach by keeping several orbitals inactive and by reducing the number of vacant orbitals in the active space. The combinations of the active space of orbitals that produced the lowest energies were finally chosen for the calculations. Excitations were not allowed from the inactive orbitals, but they were allowed to relax.

In the case of Nb_4 and Nb_4^-, $4a_1$, $3b_2$, $3b_1$, and $2a_2$ orbitals were in the active space for the C_{2v} structures, while $6a_1$, $4b_2$, $4b_1$, and $2a_2$ orbitals were kept inactive. For the pyramidal (C_s) structure, the total numbers of active and inactive orbitals were kept the same as the C_{2v} structure. The inactive orbitals in this case were composed of $10a'$ and $6a''$ orbitals, whereas the active space consisted of $7a'$ and $5a''$ orbitals. Twenty electrons (21 for Nb_4^-) were distributed among these orbitals to generate electronic states of different spin multiplicities. The final active space of Nb_5 and Nb_5^- clusters consists of $5a_1$, $4b_2$, $3b_1$, and $2a_2$ orbitals in the C_{2v} symmetry while $8a_1$, $5b_2$, $5b_1$, and $2a_2$ orbitals were kept inactive. The active space composition of the C_s structure (edge-capped tetrahedron) spans $9a'$ and $5a''$ orbitals, and the inactive space contained $13a'$ and $7a''$ orbitals. Twenty-four (25 for Nb_5^-) electrons were distributed among the active space to generate various electronic states.

The MRSDCI method of calculations was used for different electronic states of these clusters using their CASMCSCF wave functions obtained through full geometry optimization. All configurations in the CASMCSCF calculations with absolute coefficients $\geqslant 0.03$ were included as reference configurations. For the EA calculations, a smaller cutoff limit ($\geqslant 0.02$) was chosen. The CASMCSCF calculations included up to 13680 CSFs while the MRSDCI included up to 52×10^6 CSFs. The effect of unlinked quadruple clusters for the MRSDCI was estimated through a multireference Davidson correction[32] (MRSDCI+Q).

In our previous calculations on the Nb_n^+ ($n=3-5$) and Nb_3 clusters, the accuracy of the contracted $(5s3p2d)$ Gaussian basis set was tested against the original uncontracted $(5s5p4d)$ basis set as well as extended $(6s6p5d1f//6s4p4d1f)$ basis set. The geometries and energy separations of the various electronic states were found to be quite satisfactory using the $(5s3p2d)$ basis set. We have further verified the choice of the $(5s3p2d)$ basis set in the energy calculation of the anionic electronic states by calculating the energy separation of the different electronic states of Nb_4^- using the $(5s3p2d1f)$ basis set at the MRS-

TABLE I. Bond lengths $(a,b,c,\ldots)$,[a] and energy separations (ΔE) of the electronic states of Nb_4 at the CASMCSCF, MRSDCI, and MRSDCI+Q levels. The experimental ΔE values from the observed PES are included for comparison.

Structure	State	a (Å)	b (Å)	c (Å)	d (Å)	$\Delta E_{\text{CASMCSCF}}$ (eV)	ΔE_{MRSDCI} (eV)	$\Delta E_{\text{MRSDCI+Q}}$ (eV)	Expt. ΔE[b,c] (eV)
Pyramid	$^1A'$	2.713	2.483	2.601	2.568	0.10	0.00	0.00	0.0 (1.15)
(C_s)	$^1A''$	2.614	2.738	2.671	2.616	1.03	1.08	0.75	
	$^3A'$	2.454	3.283	3.169	2.498	0.00	1.28	1.60	
	$^5A'$	2.458	3.307	3.210	2.506	0.06	1.44	1.80	
	$^5A''$	2.446	3.331	3.234	2.647	0.47	1.84	2.12	
	$^3A''$	2.447	3.149	3.172	2.508	1.49	2.24	2.21	
Rhombus	^1A_g	2.507	2.847	4.128		0.69	0.67	0.64	0.45 (1.60)
(D_{2h})	$^3B_{3u}$	2.410	2.771	3.943		1.03	0.82	0.87	0.85 (2.00)
	$^3B_{2u}$	2.433	2.747	4.017		1.20	1.12	1.19	1.35 (2.50)[d]
	$^1B_{2g}$	2.410	2.766	3.947		1.85	1.22	1.10	
	$^5B_{1g}$	2.556	2.969	4.161		0.85	1.40	1.47	1.75 (2.90)[d]
	$^3B_{1g}$	2.376	2.697	3.914		1.87	1.88	2.01	1.85 (3.00)[d]
	$^5B_{3g}$	2.500	2.858	4.103		2.00	1.88	1.92	
	$^5B_1$	2.458	2.877	3.986		1.82	1.89	1.85	
	$^1B_{1g}$	2.376	2.697	3.913		1.97	1.99	2.12	2.25 (3.40)[d]
	$^1B_{2u}$	2.436	2.744	4.026		2.30	2.23	2.17	
	^5A_g	2.624	3.001	4.305		1.58	2.49	2.54	
	^3A_g	2.484	2.768	4.125		2.23	2.51	2.58	

[a]Refer to Fig. 1 for the definition of the bond lengths $(a,b,c,\ldots)$ of different structures.
[b]Reference 3.
[c]The values within parentheses indicate the actual peak positions in the PES.
[d]Alternate assignments are discussed in the text.

DCI and MRSDCI+Q levels. The agreement between the energy separations of the different electronic states in these two basis sets was quite satisfactory (discussed in detail in Sec. III C a). The B3LYP calculations were carried out using the GAUSSIAN 98 (Ref. 33) program. The CASMCSCF computations were made by GAMESS (Ref. 34) and a modified version of ALCHEMY II (Ref. 35) to include RECPs.[36] The MRSDCI calculations were carried out using ALCHEMY II.

III. RESULTS AND DISCUSSION

A. Geometries of the different electronic states of Nb_4 and Nb_5

The main objective is to determine the ground state geometries and the low-lying electronic states of these clusters. This is important to ascertain their spectroscopic properties. The analysis of the bonding characteristics of the various low-lying electronic states of Nb_4 and Nb_5 is another important objective of our studies. The equilibrium geometries and energy separations (ΔE) of the low-lying electronic states of these clusters are shown in Tables I–IV at the various level of theories.

a. Nb_4. The optimized geometries of the different electronic states of Nb_4 are listed in Table I at the CASMCSCF, MRSDCI, and MRSDCI+Q levels. The structure calculations were carried in C_{2v} (rhombus or square) and C_s (pyramidal) symmetries (Fig. 1). While the MRSDCI and MRSDCI+Q results indicate the pyramidal $^1A'$ to be the ground state, the CASMCSCF calculations favor the $^3A'$ state to be the ground state. The $^5A'$ and $^5A''$ states are very close to this ground state ($^3A'$) at the CASMCSCF level. The electronic states arising from the rhombus geometries (D_{2h}) are quite high at the CASMCSCF level while the MRSDCI and MRSDCI+Q calculations show a different trend (Table I). Since the CASMCSCF calculations were carried out in a restricted active space, and does not include dynamic-correlation effects, the ΔE values at the CASSCF level should not be considered quite accurate. The ΔE values at the MRSDCI level are more reliable as this method included dynamical electron correlation effects. Moreover, the energy separations of the various electronic states at the MRSDCI and MRSDCI+Q levels follow a similar trend. This gives further confidence in the assignment of the various electronic states using the MRSDCI level of theory.

The DFT/B3LYP optimized geometries of the various low-lying electronic states of Nb_4 are presented in Table II. Although the $^1A'$ state is the ground state, it is actually a tetrahedral structure with the T_d ($^1A_1$) symmetry. The $^3A'$ state in the C_s symmetry (pyramidal) is the next low-lying electronic state. Fowler, Garcia, and Ugalde[17] have also carried out similar DFT calculations on Nb_4 using a different ECP basis set. They have also found that the $^1A_1$ state (T_d) to be the ground state with the Nb-Nb bond lengths (2.541 Å) comparable to our results (2.538 Å). The earlier DFT calculations of Salahub[18] and Anderson *et al.*[37] gave similar results for the ground state of Nb_4, although Anderson *et al.*[37] found a slightly distorted C_{3v} structure.

The low-lying excited states in the calculation of Fowler, Garcia, and Ugalde[17] are $^3B_1$ (C_{2v},ΔE,0.44 eV), ^3A_u (D_{2h},ΔE,0.66 eV), ^3A_g (C_{2b},ΔE,1.00 eV), $^5A_1$ (C_{2v},ΔE,1.2 eV), and $^5B_1$ (C_{2v},1.38 eV) at the LSD level. A close examination of the geometries presented in Table II reveals that the $^3A'$ and $^1A''$ states are actually of C_{2v} symmetry. The ΔE and the geometry of $^3A'$ are similar to the $^3B_1$ state in the calculation of Fowler, Garcia, and Ugalde.[17] But as per our orientation it is a $^3B_2$ state. The $^3B_1$ and $^3B_2$ states in C_{2v} calculations exhibit accidental degeneracy (Table II) and are higher in energy than the $^3A'$ state.

TABLE II. Bond lengths ($a,b,c,\ldots$),[a] bond angles (θ), energy separations (ΔE), and vibrational frequencies (ν) of the electronic states of Nb_4 at the DFT/B3LYP level.

Structure	State	a (Å)	b (Å)	c (Å)	d (Å)	θ (deg)	ΔE (eV)	ν (cm^{-1})
Pyramid	$^1A'$ (T_d)[b]	2.538	2.538	2.538	2.538		0.00	162, 162, 253, 253, 253, 373
(C_s)	$^3A'$	2.495	2.884	2.495	2.555		0.46	88, 142, 217, 227, 245, 364
	$^1A''$	2.497	2.822	2.497	2.551		0.68	−63, 139, 204, 228, 233, 365
Rhombus	^1A_u	2.370	2.693	3.900			0.97	81, 136, 199, 220, 273, 331
(D_{2h})	^3A_g	2.389	2.690	3.948			1.09	−28, 137, 185, 194, 273, 324
	$^5B_{2g}$	2.413	2.785	3.941			1.52	97, 102, 188, 235, 259, 310
	$^3B_{3u}$	2.351	2.710	3.842			1.53	106, 158, 177, 218, 281, 335
	^1A_g	2.344	2.705	3.830			1.71	−215, 191, 211, 254, 258, 331
	$^3B_{1g}$	2.736	2.405	3.955			2.49	130, 188, 219, 262, 296, 316
	$^3B_{2u}$	2.346	2.675	3.855			2.58	91, 159, 191, 257, 280, 340
	$^1B_{1g}$	2.404	2.729	3.959			2.59	−85, 181, 229, 257, 303, 318
	$^1B_{2u}$	2.350	2.676	3.863			2.61	91, 163, 168, 193, 273, 336
	^5A_g	2.444	2.720	4.060			2.68	−61, 165, 192, 222, 259, 310
	$^5B_{3g}$	2.442	2.772	4.021			3.00	67, 120, 166, 259, 299, 313
	$^1B_{2g}$	2.424	2.837	3.930			3.19	−140, 189, 201, 217, 264, 298
	$^5B_{3u}$	2.455	2.743	4.074			3.45	182, 221, 242, 298, 391, 660
	$^5B_{1g}$	2.450	2.834	3.998			3.73	155, 212, 245, 264, 281, 289
	^3A_u	2.374	2.696	3.909			4.75	95, 149, 204, 234, 271, 326
D_2	^5A	2.473	2.841	2.473	2.841	70.1	1.00	133, 155, 192, 199, 200, 353
	^1A	2.520	2.568	2.833	2.568	68.4	1.22	116, 146, 208, 236, 261, 354
C_{2v}	$^1B_2$	2.417	2.797	3.904		107.7	1.59	31, 183, 248, 251, 255, 296
	$^1A_1$	2.345	2.753	3.700		104.2	1.50	82, 149, 203, 259, 285, 324
	$^3B_1$	2.405	2.952	3.491		93.1	1.56	60, 104, 143, 187, 238, 313
	$^3B_2$	2.405	2.953	3.491		93.0	1.57	60, 104, 144, 187, 238, 313
	$^5A_1$	2.429	3.114	3.114		79.7	1.58	−40, 67, 68, 124, 144, 333
	$^3A_1$	2.383	2.932	3.539		95.9	1.92	97, 173, 200, 264, 299, 320
	$^5A_2$	2.473	2.767	4.076		111.0	2.07	84, 95, 178, 204, 268, 303
	$^5B_2$	2.398	3.144	3.282		81.9	2.12	127, 139, 165, 250, 272, 309

[a]Refer to Fig. 1 for the definition of the bond lengths ($a,b,c,\ldots$) and bond angles (θ) of the different structures.
[b]The electronic state is actually $^1A_1$ in T_d symmetry.

TABLE III. Bond lengths ($a,b,c,\ldots$)[a] and energy separations (ΔE) of the electronic states of Nb_5 at the CASMCSCF, MRSDCI, and MRSDCI+Q levels. The experimental ΔE values from the observed PES are included for comparison.

Structure	State	a (Å)	b (Å)	c (Å)	d (Å)	e (Å)	f (Å)	$\Delta E_{\text{CASMCSCF}}$ (eV)	ΔE_{MRSDCI} (eV)	$\Delta E_{\text{MRSDCI+Q}}$ (eV)	Expt. ΔE[b,c] (eV)
DTB (C_{2v})	$^2A_2$	2.661	2.617	2.663	2.661	4.359		0.21	0.00	0.00	0.00 (1.65)
	$^4A_1$	2.556	2.654	2.662	2.775	4.583		0.36	0.41	0.63	0.35 (2.00)[d]
	$^4B_1$	2.846	2.388	2.582	2.794	4.405		0.26	0.43	0.63	
	$^2A_1$	2.666	2.881	2.804	2.547	4.142		0.89	0.87	0.90	
	$^6B_2$	2.507	2.513	2.784	2.791	4.765		1.17	0.91	1.20	
	$^6A_1$	2.581	2.451	2.742	2.835	4.770		0.99	1.20	1.58	1.25 (2.90)[d]
DECT (C_s)	$^2A''$	2.663	2.376	2.981	2.971	3.981	2.363	0.00	0.08	0.31	
	$^4A''$	2.489	3.040	3.055	2.803	3.985	2.398	0.90	1.04	1.37	
	$^2A'$	3.001	2.373	2.845	3.234	4.265	2.415	0.01	1.06	1.42	
	$^6A''$	2.540	3.474	3.051	2.793	4.010	2.352	1.32	1.78	2.25	
	$^4A'$	2.927	2.588	2.870	3.177	4.243	2.426	1.16	2.12	2.42	
	$^6A'$	3.137	2.350	3.046	3.111	4.204	2.402	2.70	3.96	4.41	
DTP (C_{2v})	$^4A_1$	2.878	2.788	2.554	2.921	4.125		1.08	0.73	0.70	0.75 (2.40)[d]
	$^6A_2$	3.087	2.677	2.558	2.873	4.234		0.71	1.25	1.63	
	$^2B_1$	2.857	2.668	2.572	2.909	4.201		1.14	1.47	1.80	
	$^6B_1$	2.967	2.511	2.647	3.015	4.352		1.21	1.57	1.85	1.55 (3.20)
	$^4B_2$	3.085	2.656	2.545	2.833	4.229		1.75	1.69	1.77	1.75 (3.40)[d]
	$^2B_2$	2.831	2.613	2.543	2.885	4.158		1.61	1.74	1.80	
	$^4A_2$	2.933	2.654	2.547	2.907	4.172		2.22	2.07	2.17	

[a]Refer to Fig. 1 for the definition of the bond lengths ($a,b,c,\ldots$) of different structures.
[b]From the PES of Ref. 3.
[c]The values within parentheses indicate the actual peak position the PES.
[d]The alternate assignments of the peaks are discussed in the text.

TABLE IV. Bond lengths ($a,b,c,\ldots$),[a] energy separations (ΔE), and vibrational frequencies (ν) of the electronic states of Nb_5 at the DFT/B3LYP level.

Structure	State	a (Å)	b (Å)	c (Å)	d (Å)	e (Å)	f (Å)	ΔE (eV)	ν (cm^{-1})
DTB (C_{2v})	$^2B_1$	2.644	2.899	2.641	2.512	3.988		0.0	54, 93, 116, 144, 202, 220, 260, 279, 345
	$^2A_2$	2.836	2.561	2.488	2.576	3.968		0.07	−138, 97, 118, 122, 182, 218, 264, 271, 346
	$^2A_1$	2.824	2.824	2.515	2.515	3.830		0.28	−165, −165, 87, 87, 201, 230, 230, 239, 338
	$^4B_1$	2.946	2.386	2.447	2.666	4.012		0.85	−444, −340, −93, 121, 159, 203, 274, 285, 355
	$^4A_1$	2.979	2.297	2.389	2.739	4.025		1.05	−74, 78, 145, 153, 186, 243, 269, 292, 376
	$^6A_1$	2.906	2.365	2.413	2.716	4.069		1.25	−190, 90, 137, 153, 181, 237, 258, 351, 1857
	$^6B_2$	2.916	2.412	2.397	2.680	3.996		1.44	52, 141, 145, 176, 261, 275, 340, 341, 368
DECT (C_s)	$^2A'$	2.512	2.643	2.645	2.901	3.990	2.513	0.04	55, 95, 116, 144, 202, 220, 255, 280, 345
	$^4A''$	2.521	2.597	2.640	3.012	3.932	2.522	0.48	−121, 120, 137, 160, 198, 207, 213, 266, 332
	$^4A'$	2.570	2.515	2.568	2.995	4.048	2.480	0.88	−286, 113, 126, 128, 191, 213, 227, 255, 339
	$^6A''$	2.502	2.575	2.792	2.963	3.823	2.503	1.09	94, 103, 151, 157, 177, 200, 212, 266, 325
DTP (C_{2v})	$^2B_2$	2.785	2.550	2.516	2.926	4.077		0.42	−99, 128, 170, 172, 204, 219, 242, 248, 340
	$^2B_1$	2.746	2.532	2.530	3.005	4.053		0.94	−112, 126, 128, 172, 194, 214, 227, 235, 333
	$^4A_2$	2.857	2.573	2.482	2.880	4.037		1.03	−96, 121, 188, 200, 209, 223, 240, 330, 409
	$^6A_2$	2.692	2.553	2.587	2.869	4.216		1.07	−87, 68, 110, 121, 183, 192, 197, 209, 340
	$^6B_1$	2.737	2.593	2.565	3.022	4.013		1.76	−127, 104, 114, 157, 177, 178, 209, 239, 330
	$^4A_1$	2.696	2.513	2.611	3.015	4.212		1.98	−142, 57, 113, 158, 166, 183, 183, 211, 333
	$^4B_2$	2.808	2.527	2.577	2.842	4.268		2.09	−87, 100, 108, 137, 144, 199, 207, 291, 325
	$^2A_2$	2.707	2.502	2.589	3.022	4.169		3.46	−166, −102, 126, 166, 178, 189, 236, 335, 848

[a]Refer to Fig. 1 for the definition of the bond lengths ($a,b,c,\ldots$) of different structures.

These C_{2v} structures ($^3B_1$ and $^3B_2$) have actually been encompassed into local minima during geometry optimization and are high-energy geometries. The ^3A_g state has a similar ΔE value compared to the result of Fowler, Garcia, and Ugalde[17] while ^3A_u could not be identified in the low-energy region in our calculation (Table II). The $^1A''$ state that actually has a C_{2v} structure ($^1B_1$) is 0.68 eV above the ground state. All the other singlet C_{2v} states are higher in energy (Table II).

We have identified a few other low-lying excited states, viz., $^5A\,(D_2)$, $^1A\,(D_2)$ (Fig. 1), and $^1A_u\,(D_{2h})$ within 1.2 eV energy separation of the ground state. These low-lying excited states were not reported in the previous DFT calculations.[17] The $^5A_1$ structure (C_{2v}) in our calculation is higher in energy than that of Fowler, Garcia, and Ugalde[17] and we have not identified the higher energy $^5B_1$ (C_{2v}) state in our calculation. Thus the main features of our DFT excited states are similar to those of Fowler, Garcia, and Ugalde[17] The differences, which are observed regarding the assignments of a few higher energy states, could arise from the use of different ECP basis set in our calculations.

The ΔE values obtained for the different electronic states at the MRSDCI and MRSDCI+Q levels exhibit remarkable differences from those obtained at the DFT/B3LYP level. The C_s structures obtained at the CASMCSCF/MRSDCI level are mostly distorted. We shall show in the following section that these structural distortions occur due to the Jahn-Teller effect. The other factor is the multireference nature of the wave functions of the different electronic states at CASMCSCF/MRSDCI level. The correlation effect arising from this multireference character is not accountable in the single reference treatment, and the observed ΔE values in the MRSDCI calculations are mostly the result of this effect.

The first excited low-lying electronic state in the DFT/B3LYP calculation is $^3A'$. This electronic state is 1.28 eV above the ground state at the MRSDCI (1.60 eV in MRSDCI+Q) level. The leading electronic configurations of the $^3A'$ state ($36\%|1a'^2\cdots15a'^216a'^117a'^11a''^2\cdots9a''^210a''^2\rangle+22\%|1a'^2\cdots15a'^216a'^217a'^21a''^2\cdots9a''^110a''^1\rangle+\cdots$) show that this state is arising from the $^1A''$ ($67\%|1a'^2\cdots15a'^216a'^217a'^11a''^2\cdots9a''^210a''^1\rangle$) state through excitation of $16a'$ (or $9a''$ for second leading configuration) electron. Now, the $^1A''$ state is the higher energy Jahn-Teller component of the $^1A'$ ground state. Thus the $^3A'$ state has quite a high ΔE value.

The first low-lying ^1A_g excited state at the CASMCSCF/MRSDCI level ($\Delta E=0.67$ eV) is quite high at the DFT/B3LYP level. The ^1A_g electronic state is highly multireference in nature ($43\%|1a_g^2\cdots7a_g^21b_{1u}^2\cdots3b_{1u}^21b_{2u}^2\cdots\times4b_{2u}^21b_{3g}^21b_{3u}^2\cdots5b_{3u}^21b_{2g}^22b_{2g}^21b_{1g}^2\cdots3b_{1g}^21a_u^2\rangle+18\%|1a_g^2\cdots7a_g^21b_{1u}^2\cdots3b_{1u}^21b_{2u}^2\cdots4b_{2u}^21b_{3g}^22b_{3g}^21b_{3u}^2\cdots5b_{3u}^21b_{2g}^22b_{2g}^21b_{1g}^2\cdots3b_{1g}^2\rangle+10.3\%|1a_g^2\cdots6a_g^21b_{1u}^2\cdots3b_{1u}^21b_{2u}^2\cdots5b_{2u}^21b_{3u}^2\cdots5b_{3u}^21b_{2g}^22b_{2g}^21b_{1g}^2\cdots3b_{1g}^21a_u^2\rangle+4.4\%|1a_g^2\cdots7a_g^21b_{1u}^2\cdots3b_{1u}^21b_{2u}^2\cdots4b_{2u}^21b_{3g}^21b_{3u}^2\cdots5b_{3u}^21b_{2g}^22b_{2g}^21b_{1g}^2\cdots3b_{1g}^21a_u^2\rangle+\cdots$). The high correlation effect arising from the multireference effect gives the ^1A_g state enhanced stability over the other states. This effect could not be noticed in any single reference calculations.

b. Nb_5. The optimized geometries and energy separations for the various electronic states of the Nb_5 cluster in distorted tetragonal pyramid (DTP), distorted trigonal bipyramid (DTB) and distorted edge-capped tetrahedron (DECT) structures are shown in Table V at the CASMSCF, MRSDCI, and MRSDCI+Q levels. The optimized minimum energy geometry of each cluster is shown in Fig. 2. The important feature of the trigonal bipyramid and tetragonal pyramid structures is that the structures do not retain perfect D_{3h} and C_{4v} symmetries during geometry optimization. The edge-capped tetrahedral structure also distorts from its ideal

TABLE V. Bond lengths ($a,b,c,\ldots$),[a] relative energies (ΔE) of the $^1E'$, $^1A'$, and $^1A''$ states of Nb_4 (at the DFT/B3LYP and MRSDCI levels), and the $^2E''$, $^2A_2$, and $^2B_2$ states of Nb_5 (DFT/B3LYP level).

Cluster	Method	State	a (Å)	b (Å)	c (Å)	d (Å)	e (Å)	ΔE (eV)
Nb_4	DFT/B3LYP	$^1A'$	2.538	2.538	2.538	2.538		0.00
		$^1A''$	2.497	2.822	2.497	2.551		0.68
		^1E	2.566	2.566	2.566	2.566		2.50
	MRSDCI	$^1A'$	2.713	2.483	2.601	2.568		0.00
	(MRSDCI+Q)							(0.00)
	MRSDCI	$^1A''$	2.614	2.738	2.671	2.616		1.08
	(MRSDCI+Q)							(0.75)
	MRSDCI	^1E[b]	2.597	2.597	2.597	2.597		1.09[c] (1.14)[d]
	(MRSDCI+Q)							0.78[c] (0.81)[d]
Nb_5	DFT/B3LYP	$^2B_1$	2.644	2.899	2.641	2.512	3.988	0.00
		$^2A_2$	2.836	2.561	2.488	2.576	3.968	0.07
		$^2E''$	2.621	2.621	2.621	2.621	4.279	1.29

[a]Refer to Fig. 1 for the definitions of a, b, c,... .
[b]The geometry of this state has been optimized at the MRSDCI level.
[c]ΔE calculated from $^1A''$.
[d]ΔE calculated from $^1A'$.

C_{2v} structure. So the various electronic states of the DTP and DTB structures are assigned in the C_{2v} symmetry, whereas the electronic states of the DECT structure are assigned in the C_s symmetry. The $^2A_2$ state of the DTB structure was found to be the minimum at the MRSDCI level. This is not an unambiguous ground state, as the $^2A''$ electronic state of the DECT structure is just 0.08 eV (0.31 eV at the MRSDCI+Q level) above the $^2A_2$ ground state (Table III).

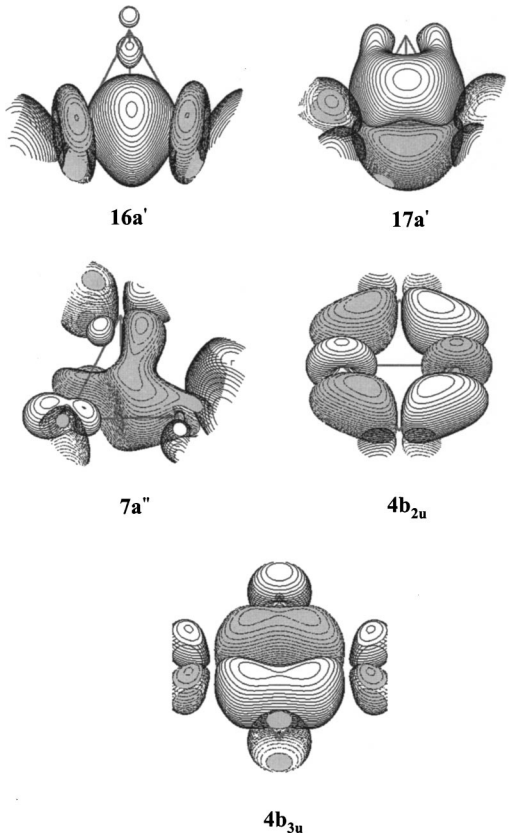

FIG. 2. The active space MOs of the ground ($^1A',C_s$) and the first excited state ($^1A_g,D_{2h}$) of Nb_4. Only a few selected MOs of these two electronic states [$16a'$, $17a'$, $7a''$ ($^1A'$), $4b_{2u}$, and $4b_{3u}$ (^1A_g)], calculated at the CAMCSCF/MRSDCI level, are presented here. The pictures were originally drawn keeping z as the vertical axis. Each MO picture is then rotated to have better visualization.

The triangular base formed by the Nb_1, Nb_2, and Nb_3 atoms [Fig. 1(d)] of the DTB structure constitutes an isosceles triangle. Thus we have two different types of axial-equatorial distances [distances c and d in Fig. 1(f)] due to isosceles triangular arrangement of the base. As seen from Table V, there is considerable difference between the two equal sides of the isosceles triangle relative to the third side. This, together with energy separations presented in Table V, suggests that the Jahn-Teller distortion is considerable in these structures. The MRSDCI energy separations indicate that electronic states of the DTB structure are lower in energy (Table III).

The energies of the various electronic states of the DTP structure (Table III) indicate that apart from the $^4A_1$, $^6A_2$, $^2B_1$ states, all other electronic states are higher in energy. The geometries of the different electronic states of the DTP structure indicate that although the distances among four Nb atoms forming the tetragonal base are the same, they are not in the same plane. That is, they form a puckered structure to avoid steric strain [Fig. 1(e)]. This makes the distances a and b unequal for all the electronic states of the DTP structure presented in Table III. If the distortion of the structures is too high, they could be converted into the DTB structure during optimization, if the corresponding DTB electronic state is lower in energy. Thus all four electronic states (viz., $^nA_1$, $^nB_2$, $^nB_1$, and $^nA_2$) in a particular spin state n ($n=2,4,6$) could not be found in the DTB or DTP structures. Table V also contains the geometries and ΔE of the various electronic states of the DECT structure of Nb_5 at the CASMCSCF, MRSDCI, and MRSDCI+Q levels. The results indicate that the $^2A''$, $^4A''$, and $^2A'$ states are the low-lying excited states (within ΔE of 1.1 eV), whereas the $^6A''$, $^4A'$, and $^6A'$ electronic states of this cluster are considerably higher.

The earlier DFT calculations of Goodwin and Salahub[18] pointed that a doublet trigonal bipyramid structure is the

ground state of Nb_5. They did not suggest any assignment for the electronic state and found that the ionization of the cluster leads to a Jahn-Teller distorted trigonal bipyramid. The results of our DFT/B3LYP calculations on the different electronic states of Nb_5 are presented in Table IV. The results indicate a $^2B_1$ state with the DTB geometry as the ground state. The $^2A_2$ (DTB) state is assigned as ground state at the MRSDCI and MRSDCI+Q levels while the $^2A'$ (DECT) state is nearly degenerate. As would be seen in the following section, the $^2A_2$ (DTB) state undergoes Jahn-Teller distortion and the MRSDCI calculation predicts the state to be lower-energy Jahn-Teller component of the $^2E''$ state. In the present DFT/B3LYP calculation, the observed Jahn-Teller energy separation between the $^2B_1$ and $^2A_2$ components is quite low and the $^2B_1$ state is the lower-energy component. The MRSDCI wave function of the $^2A_2$ (DTB) state is highly multireference in character $(66\%|1a_2\cdots 13a_1^2 1b_2^2\cdots 9b_2^2 1b_1^2\cdots \times 7b_1^2 1a_2^2\cdots 3a_2^2 4a_2^1\rangle + 2.3\%|1a_2\cdots 13a_1^2 1b_2^2\cdots 9b_2^2 1b_1^2\cdots \times 7b_1^1 8b_1^1 1a_2^2\cdots 3a_2^2\rangle + 1.44\%|1a_2\cdots 14a_1^2 1b_2^2\cdots 8b_2^2 1b_1^2\cdots \times 7b_1^2 1a_2^2\cdots 3a_2^2 4a_2^1\rangle + 1\%|1a_2\cdots 13a_1^2 14a_1^1 1b_2^2\cdots \times 8b_2 9b_2^1 1b_1^2\cdots 6b_1^2 7b_1^1 1a_2^2\cdots 4a_2^1\rangle + \cdots)$. The $^2B_1$ (DTP) structure, on the other hand, has only two dominant configurations $(67\%|1a_2\cdots 13a_1^2 1b_2^2\cdots 9b_2^2 1b_1^2\cdots 7b_1^2 8b_1^1 1a_2^2\cdots \times 3a_2^2\rangle + 1.44\%|1a_2\cdots 14a_1^2 1b_2^2\cdots 8b_2^2 1b_1^2\cdots 7b_1^2 8b_1^1 1a_2^2\cdots \times 3a_2^2\rangle + \cdots)$. Apart from the higher stabilization due to electron correlation effect in the $^2A_2$ state, the $^2B_1$ state could be thought to be an excited state through excitation from $4a_2$ to $8b_1$ orbitals. In fact, the Jahn-Teller stabilization of the $^2A_2$ state is quite large at the MRSDCI level. The DFT/B3LYP results further show that the $^2A_1$ and $^4B_1$ states of the DTB structure are low-lying electronic states. The results are similar to those of the MRSDCI and MRSDCI+Q, although their ΔE's differ.

B. Nature of geometric distortions in the low-lying electronic states of Nb_4 and Nb_5

Most of the electronic states of Nb_4 in C_s symmetry undergo distortions from ideal tetrahedral structures (T_d), including the ground state ($^1A'$), at the CASMCSCF/MRSDCI level (Table I). The $^1A'$ ground state has the same electronic configuration $(1a'^2\cdots 17a'^2 1a''^2\cdots 9a''^2)$ at the DFT/B3LYP and CASMCSCF/MRSDCI levels. But this state has the ideal tetrahedral structure with the T_d ($^1A_1$) symmetry at the DFT/B3LYP level. The leading configuration contributes only 69% to the total wave function at the CASMCSCF/MRSDCI level. Thus, the multireference character of the wave function plays an important role in the distortion of the $^1A'$ state.

To verify the nature of distortion at the CASMCSCF/MRSDCI level, we have optimized the geometry of the $^1A'$ state in a perfect T_d symmetry. The leading configuration of this state in the T_d group $(\cdots a_1^2 a_1^2 t_2^4 t_2^4 e^4 t^2 e^2)$ shows that this electronic state is ^1E. Thus, the ^1E state would undergo Jahn-Teller distortion into the $^1A'$ and $^1A''$ states that we have calculated at the CAMCSCF/MRSDCI level. This is also true for the other electronic states of Nb_4 in the C_s symmetry. We have further checked this case by calculating the energy of the ^1E state from both $^1A'$ and $^1A''$ states and the energies differ only by 0.05 eV at the MRSDCI and 0.03 eV at the MRSDCI+Q level (Table V). Evidently, the $^1A'$ and $^1A''$ states (T_d symmetry) correlate into the ^1E state and the energy of the ^1E state is higher than either of the $^1A'$ (ground state) and $^1A''$ states in the C_s symmetry. This is an ideal example of geometric distortion occurring through $T\otimes e$ Jahn-Teller effect, as discussed in Bersuker's review.[23]

The discrepancy between the DFT/B3LYP and CSMCSCF/MRSDCI results needs to be discussed further. Table V contains the energies of the optimized geometries of the ^1E state together with the $^1A'$ and $^1A''$ states at the DFT/B3LYP level. The results indicate that the energy of the ^1E state is higher than the $^1A'$ and $^1A''$ states. Note that the A' (C_s) state correlates with the A_1 and E states in T_d symmetry. Likewise, the A'' representation correlates into the A_2 and E states. The computed energy values indicate that ^1E is a higher root at the DFT/B3LYP level. Since this state is really multireference in character, it appears to become a lower root at the CASMCSCF/MRSDCI level due to the electron correlation effects. Thus the ground state of Nb_4 is an undistorted T_d structure ($^1A_1$) at the DFT/B3LYP level. The planar structures of Nb_4 in their different electronic states are all D_{2h} in nature at both the DFT/B3LYP and CASMCSCF/MRSDCI levels. These structures are distorted from their ideal D_{4h} (square) structures. The distortions of the B_{2u}, B_{3u}, B_{3g}, and B_{2g} states of the D_{4h} structure fall under the $E\otimes b_1$ type Jahn-Teller coupling. This is a special case $E\otimes(b_1+b_2)$ distortion,[23] where the b_1 distortion transforms a square into a rhombus. The structural distortions of the rest of the electronic states are not of Jahn-Teller origin.

The ground state of Nb_5 ($^2A_2$,DTB) is a distorted structure from an ideal D_{3h} symmetry at the CASMCSCF/MRSDCI level. This state competes for the ground state at the DFT/B3LYP level. The ground state at the DFT/B3LYP level ($^2B_1$) is only 0.07 eV lower and both the states have distorted D_{3h} structures. The ideal D_{3h} structure of $^2A_2$ has the $e''^2 a_1''^1$ electronic configuration at the CASMCSCF/MRSDCI level. This means that this state in D_{3h} symmetry is $^2E''$. Thus, the $^2A_2$ state is distorted due to the Jahn-Teller effect ($E\otimes e$ type Jahn-Teller effect[23]). The DFT/B3LYP results also show that the $^2B_1$ and $^2A_2$ states are Jahn-Teller components. Table V contains the energies of these two states ($^2B_1$ and $^2A_2$) together with the energy of the $^2E''$ (D_{3h}) state at the DFT/B3LYP level. The energy separation between the two Jahn-Teller components is very small. It has been shown in the preceding section that the electron correlation effects due to multireference nature of these two states increase the energy separation between them at the MRSDCI and MRSDCI+Q levels. Since the reaction coordinate separating the geometries between the DTB and DTP structures is the simple bending mode containing the plane Nb_2-Nb_4-Nb_3-Nb_5 [Figs. 1(d) and 1(e)], the higher energy $^2B_1$ is distorted to the DTP structure. The distortions of the other electronic states of the DTP and the DTB structures could be similarly explained.

TABLE VI. Bond lengths ($a,b,c,\ldots$),[a] and energy separations (ΔE) of the electronic states of Nb_4^- at the MRSDCI, and MRSDCI+Q levels. The optimized geometric parameters presented here are at the CASMCSCF level.

Structure	State	a (Å)	b (Å)	c (Å)	d (Å)	ΔE_{MRSDCI}[b] (eV)	$\Delta E_{\text{MRSDCI+Q}}$[b] (eV)
Rhombus (D_{2h})	$^2B_{3g}$	2.318	2.608	3.869		0.00 (0.00)	0.00 (0.00)
	$^4B_{1u}$	2.365	2.705	3.881		0.17 (0.42)	0.23 (0.50)
	$^4B_{2g}$	2.290	2.607	3.767		0.30 (0.28)	0.36 (0.31)
	$^2B_{1u}$	2.356	2.688	3.869		0.76 (0.62)	0.81 (0.72)
	^4A_u	2.324	2.682	3.795		0.62 (1.02)	0.73 (1.12)
	$^2B_{1g}$	2.383	2.651	3.960		1.02 (1.14)	1.07 (1.19)
	$^2B_{3u}$	2.452	2.941	3.926		1.31 (1.85)	1.34 (1.77)
Pyramid (C_s)	$^2A''$	2.403	3.086	3.204	2.430	0.49 (1.57)	0.84 (2.02)
	$^2A'$	2.418	3.228	3.138	2.401	0.49 (1.60)	0.86 (2.09)
	$^4A'$	2.422	3.241	3.241	2.422	0.77 (1.82)	1.19 (2.33)
	$^4A''$	2.381	3.249	3.095	2.517	1.47 (2.50)	1.87 (3.03)

[a]Refer to Fig. 1 for the definition of the bond lengths ($a,b,c,\ldots$) of different structures.
[b]The ΔE values within parentheses are calculated using ($5s5p4d1f//5s3p2d1f$) basis set while the ΔE values without parentheses were calculated using ($5s5p4d//5s3p2d$) basis set of Nb.

C. Electronic structures of Nb_4^- and Nb_5^- in their ground and excited states

We have computed the properties of the anions to facilitate the assignment of the observed PES.[3] The energy separations of the different electronic states of Nb_4^- have been determined using two different basis sets of Nb ($5s5p4d1f//5s3p2d1f$) and ($5s5p4d//5s3p2d$) at the MRSDCI and MRSDCI+Q levels. This facilitates to calibrate the accuracy of our calculations.

a. Nb_4^-. The optimized geometries and the energy separations of the different low-lying electronic states of Nb_4^- are shown in Table VI at the CASMCSCF, MRSDCI, and MRSDCI+Q levels. Since the CASMCSCF energy separations in the restricted active space calculations are not reliable (discussed in the previous section), the ΔE values are presented at the MRSDCI and MRSDCI+Q levels only. The results in Table IV indicate that the ground state of Nb_4^- has a rhombus structure ($^2B_{3g}$). The energy separations of the various low-lying electronic states are similar in the smaller ($5s5p4d//5s3p2d$) and larger ($5s5p4d1f//5s3p2d1f$) basis sets. Only for the $^2A''$ and $^2A'$ states of the C_s structure, the larger basis set calculations yield higher energy separations. But both the basis sets do not yield these electronic states as the ground states at the MRSDCI and MRSDCI+Q

TABLE VII. Bond lengths ($a,b,c,\ldots$),[a] energy separations (ΔE), and vibrational frequencies (ν) of the electronic states of Nb_4^- at the DFT/B3LYP level.

Structure	State	a (Å)	b (Å)	c (Å)	d (Å)	ΔE (eV)	ν (cm^{-1})
Pyramid (C_s)	$^2A'$	2.491	2.484	2.491	2.580	0.0	42, 151, 158, 232, 234, 351
	$^2A''$	2.756	2.265	2.611	2.290	0.32	−142, 120, 149, 168, 297, 362
	$^4A'$	2.648	2.435	2.489	2.407	0.41	−124, 115, 198, 240, 352, 377
	$^4A''$	2.544	2.526	2.548	2.366	0.44	
Rhombus (D_{2h})	$^2B_{1g}$	2.342	2.629	3.875		0.19	70, 110, 205, 240, 274, 325
	$^4B_{2g}$	2.324	2.639	3.825		0.26	110, 124, 201, 210, 282, 331
	$^2B_{1u}$	2.317	2.629	3.817		0.97	132, 154, 181, 207, 261, 325
	$^2B_{3g}$	2.321	2.618	3.834		1.26	125, 175, 197, 207, 279, 331
	$^4B_{1u}$	2.411	2.633	4.040		1.60	
	$^4B_{3u}$	2.359	2.665	3.893		1.94	130, 162, 248, 261, 318, 348
	$^2B_{3u}$	2.361	2.659	3.901		2.01	83, 154, 248, 257, 307, 319
	^4A_u	2.413	2.875	3.876		2.06	−139, 199, 208, 291, 355, 404

[a]Refer to Fig. 1 for the definition of the bond lengths ($a,b,c,\ldots$) of different structures.

TABLE VIII. Bond lengths ($a,b,c,\ldots$),[a,b] and energy separations (ΔE) of the electronic states of Nb_5^- at the MRSDCI and MRSDCI+Q levels. The optimized geometries presented here were calculated at the CAMCSCF level.

Structure	State	a (Å)	b (Å)	c (Å)	d (Å)	e (Å)	f (Å)	$\Delta E_{\mathrm{MRSDCI}}$ (eV)	$\Delta E_{\mathrm{MRSDCI+Q}}$ (eV)
DTB (C_{2v})	$^3B_1$	2.858	2.249	2.449	2.753	4.208		0.00	0.002
	$^1A_1$	2.746	2.867	2.315	2.746	2.867		0.04	0.00
	$^1B_1$	2.858	2.241	2.459	2.762	4.233		0.16	0.19
	$^3A_2$	2.879	2.226	2.464	2.771	4.238		0.19	0.21
	$^3B_2$	2.877	2.263	2.511	2.739	4.249		0.19	0.28
	$^1A_2$	2.877	2.224	2.454	2.773	4.241		0.22	0.25
DTP (C_{2v})	$^3A_1$	2.741	2.943	2.294	2.741	2.943	3.983	0.19	0.17
	$^1B_2$	2.731	3.069	2.245	2.731	3.069	4.043	0.23	0.23
DECT (C_s)	$^3A''$	2.362	2.918	2.720	2.799	4.012	2.532	0.78	0.75
	$^1A''$	2.448	2.455	2.838	2.828	4.011	2.489	1.10	1.03
	$^3A'$	2.438	2.428	3.049	2.781	4.036	2.479	1.37	1.28
	$^1A'$	2.746	2.226	2.976	2.266	4.113	2.678	1.63	1.83

[a]Refer to Fig. 1 for the definition of the bond lengths ($a,b,c,\ldots$) of different structures.

levels. However, the results of the DFT/B3LYP calculations (Table VII) differ from those of the MRSDCI and MRSDCI+Q results. Although the DFT/B3LYP calculations predict the rhombus structures as the low-lying electronic states, the ground state is a pyramidal (C_s,$^2A'$) structure at the DFT level. The previous LSD calculations by Fournier, Pang, and Chen[20] have also predicted that the ground state of Nb_4^- is a pyramidal doublet structure.

The $^2B_{3g}$ ground state structure of Nb_4^- is a Jahn-Teller distorted structure ($E\otimes b_1$ type[23]) and is of multireference character ($73\%|1a_g^2\cdots 7a_g^2 1b_{1u}^2\cdots 3b_{1u}^2 1b_{2u}^2\cdots 4b_{2u}^2 1b_{3g}^2 \times 2b_{3g}^1 1b_{3u}^2\cdots 5b_{3u}^2 1b_{2g}^2 2b_{2g}^2 1b_{1g}^2\cdots 3b_{1g}^2 1a_u^2\rangle + 2.3\%| \times 1a_g^2\cdots 7a_g^2 1b_{1u}^2\cdots 3b_{1u}^2 1b_{2u}^2\cdots 4b_{2u}^2 b_{3g}^2 2b_{3g}^1 1b_{3u}^2\cdots \times 5b_{3u}^2 1b_{2g}^2 2b_{2g}^2 1b_{1g}^2\cdots 3b_{1g}^2 1a_u^1 2a_u^1\rangle + \cdots$). The $^2A'$ state is also multireference character ($60\%|1a'^2\cdots \times 16a'^2 17a'^2 1a''^2\cdots 10a''^2\rangle + 16\%|1a'^2\cdots 16a'^2 17a'^2 1a''^2 \times\cdots 10a''^1 11a''^1\rangle + \cdots$) at the CASMCSCF/MRSDCI level. Thus electron correlation stabilization effects are important for both the electronic states. The extra stabilization of the $^2B_{3g}$ state could be explained from the ease of formation of the Nb_4 ground state through electron detachment. An examination of the leading electronic configuration of the $^1A'$ ground state of Nb_4 ($1a'^2\cdots 16a'^2 17a'^2 1a''^2\cdots 9a''^2$) shows that it cannot be formed from the $^2A'$ state through a simple electron detachment from a' or a'' orbitals. This process more likely results in the $^1A''$ state of Nb_4, which is 1.08 eV above the Nb_4 ground state ($^1A'$). On the other hand, the leading electronic configuration of the ground state of Nb_4^-($^2B_{3g}$) shows that it correlates with the $1a'^2\cdots 16a'^2 17a'^2 1a''^2\cdots 10a''^1$ configuration in the C_s symmetry. The $^1A'$ state is easily formed through this state by an electron detachment to the $10a''$ (b_{3g}) orbital and thus the ^3B_g state should have higher stabilization with respect to the $^2A'$ state.

b. Nb_5^-. The geometries and the energies of the various low-lying electronic states of Nb_5^- are presented in Table VIII at the CASMCSCF, MRSDCI, and MRSDCI+Q levels. The optimized geometries are at the CASMCSCF level while the ΔE values are presented at the MRSDCI and MRSDCI+Q levels. The ground state of Nb_5^- varies as a function of level of theory. The $^3B_1$ and $^1A_1$ states of the DTB structure compete as a candidate for the ground state. The DFT/B3LYP results of the different electronic states of Nb_5^- (Table IX) also show that the ground state of the anion is sensitive to the level of theory. Here three electronic states of the DTB structure, viz., $^1A_1$, $^3A_2$, and $^1A_2$ compete for the ground state. The $^3A_2$ and $^1A_2$ electronic states are low-lying states at the MRSDCI and MRSDCI+Q levels, but their energy separations are slightly higher (Table IX). The

TABLE IX. Bond lengths ($a,b,c,\ldots$),[a] energy separations (ΔE), and vibrational frequencies (ν) of the electronic states of Nb_5^- at the DFT/B3LYP level.

Structure	State	a (Å)	b (Å)	c (Å)	d (Å)	e (Å)	f (Å)	ΔE (eV)	ν (cm^{-1})
DTB (C_{2v})	$^1A_1$	2.744	2.745	2.470	2.470	3.790		0.00	77, 77, 116, 116, 242, 242, 246, 262, 328
	$^3A_2$	2.840	2.431	2.431	2.553	3.899		0.04	−103, 116, 116, 129, 181, 218, 262, 264, 335
	$^1A_2$	2.836	2.431	2.431	2.555	3.905		0.07	−57, 112, 129, 129, 181, 220, 264, 272, 335
	$^3B_2$	2.852	2.453	2.352	2.583	3.840		0.23	90, 125, 177, 182, 193, 268, 283, 322, 337
	$^1B_1$	2.926	2.350	2.366	2.617	3.866		0.66	−115, 65, 162, 171, 218, 270, 273, 335, 582
	$^3A_1$	2.766	2.927	2.487	2.485	3.754		1.57	−283, −75, 109, 130, 215, 229, 264, 269, 315
DTP (C_{2v})	$^1B_2$	2.599	2.655	2.455	2.797	3.892		0.28	92, 106, 118, 142, 200, 235, 269, 308, 329
	$^3B_1$	2.672	2.577	2.457	2.871	3.934		0.55	−47, 112, 133, 142, 200, 235, 269, 308, 329
DECT (C_s)	$^1A'$	2.490	2.618	2.538	2.975	3.938	2.489	0.55	32, 73, 131, 187, 236, 239, 251, 278, 334
	$^3A'$	2.497	2.514	2.656	2.973	3.843	2.498	0.81	−20, 98, 102, 165, 164, 188, 220, 265, 326
	$^1A''$	2.567	2.442	2.568	2.938	3.960	2.371	1.26	−105, 98, 110, 121, 184, 191, 232, 257, 311

[a]Refer to Fig. 1 for the definition of the bond lengths ($a,b,c,\ldots$) of different structures.

TABLE X. Calculated electron affinity (EA), ionization potential (IP), dissociation energy (D_e, including the value of the corresponding cation), and atomization energy (AE, per atom) of Nb_4 and Nb_5 at the various levels of theory. Experimental data are also included in the table for comparison. The parameters, if not indicated, are calculated using ($5s5p4d//5s3p2d$) basis set of Nb.

	Nb_4				Nb_5				D_e (cations)	
Method	EA (eV)	IP (eV)	D_e (eV)	AE (eV)	EA (eV)	IP (eV)	D_e (eV)	AE (eV)	Nb_4^+	Nb_5^+
MRSDCI	1.24[a]	5.60[b] (4.77[c],4.33[a])	6.02	3.68	1.54[b]	5.39[b]	5.58	4.06	5.85	5.79
MRSDCI+Q	1.42[a]	5.76[b] (4.96[c],4.56[a])	6.79	3.88	1.58[b]	5.71[b]	6.25	4.36	6.64	6.30
DFT/B3LYP	0.82[d]	5.43[d]	6.07[d]	4.32[d]	1.31[d]	5.22[d]	5.51[d]	4.56[d]		
	(0.824)[e]	(5.44)[e]	(6.10)[e]		(1.32)[e]	(5.23)[e]	(5.53)[e]			
Experimental	1.15[f]	5.64±0.005[g]	5.9±0.80[h]	3.84[j]	1.65[f]	5.45±0.05[g]	5.35±0.2[h]	4.14[j]	5.900±0.2[b]	5.50±0.2[b]
		5.58±0.1[h]	6.26±0.72[i]	4.29[j]		5.43±0.05[h]	5.46±0.29[i]	4.52[j]	6.00±0.3	5.61±0.3[i]
		5.80±0.31[i]								

[a]Calculated using ($5s5p4d1f//5s3p2d1f$) basis set of Nb.
[b]Calculated using thermodynamic cycle (see the text for details).
[c]Calculated using ($6s6p4d//6s4p3d$) basis set of Nb.
[d]Calculated using ($6s6p5d1f//6s4p4d1f$) basis set of Nb.
[e]Calculated using ($6s6p5d1f1g//6s4p4d1f1g$) basis set of Nb.
[f]Reference 3.
[g]Reference 39.
[h]Reference 17.
[i]Reference 6.
[j]Calculated using the experimental D_e values in Refs. 5 and 6.

$^3B_1$ state at the DFT/B3LYP level has a DTP structure and its energy is slightly higher. At the CASMCSCF/MRSDCI level both the $^3B_1$ and $^3A_2$ states exhibit DTB equilibrium structures and undergo Jahn-Teller distortion. The $^3B_1$ state in this case is the lower energy component of the $^3E''$ (D_{3h}) state.

The CASMCSCF/MRSDCI leading electronic configurations of the $^3B_1$ ($1a_1^2\cdots14a_1^21b_2^2\cdots8b_2^29b_2^11b_1^2\cdots8b_11a_2^2\cdots3a_2^24a_2^1$) and $^1A_1$ ($1a_1^2\cdots13a_1^21b_2^2\cdots9b_2^21b_1^2\cdots7b_11a_2^2\cdots4a_2^2$) electronic states of Nb_5^- indicate that the generation of the Nb_5 ground state ($^2A_2$,$1a_1^2\cdots13a_1^21b_2^2\cdots9b_2^21b_1^2\cdots7b_11a_2^2\cdots3a_2^24a_2^1$) through electron detachment is more feasible from the $^1A_1$ ground state. Thus the preferred ground state of Nb_5^- should be $^1A_1$. The present DFT/B3LYP results and the previous LSD calculations by Fournier, Pang, and Chen[20] also support this ground state assignment.

D. Vibrational frequencies of the Nb_n and Nb_n^- (n=4,5) clusters

Tables II, IV, VII, and IX list the vibrational frequencies of the different electronic states of Nb_4, Nb_4^-, Nb_5, and Nb_5^-, respectively. The calculated frequencies of most of the low-lying electronic states are all positive and thus confirming that the calculated geometries are true minima on the energy surfaces. There are few cases for which one of the frequencies has a low imaginary value. Since the available PES of Nb_n clusters[3] are not vibrationally resolved, the calculated vibrational spectra of the Nb_n and Nb_n^- (n=4,5) cannot be compared with any experimental values.

Fournier, Pang, and Chen[20] have previously calculated the vibrational frequencies (ν) of the Nb_n^- (n=4,5) clusters using the LSD technique and have found that the frequencies of the anionic clusters are not much different from the neutral clusters. Our present DFT/B3LYP calculations show that the symmetric stretching frequencies of Nb_4 and Nb_5 are around 360–373 and 328–335 cm^{-1}, respectively. In our previous work on Nb_n^+ (n=3–5) clusters,[31] it was found that the symmetric stretching modes of the ground electronic states roughly correlate with their dissociation energies. The calculated ground state symmetric stretching modes of Nb_4^+ ($^2A'$) and Nb_4 ($^1A'$) are 361 and 373 cm^{-1}, respectively. Similar values for the Nb_5^+ ($^3A_1$,DTP) and Nb_5 ($^2A_2$,DTB) are 356 and 345 cm^{-1}. The experimental dissociation energies[5,6] (D_e) of Nb_4^+, Nb_4, Nb_5^+, and Nb_5 are 5.9, 5.64, 5.5, and 5.35 eV, respectively. These results show that the relative stabilities of the cationic and neutral clusters cannot be predicted solely from their symmetric stretching modes. This was also the case for the Nb_3 and Nb_3^+ clusters. But if we compare the symmetric stretching modes of the Nb_3 (ν, 326 cm^{-1}; D_e, 5.01 eV), Nb_4, and Nb_5 with their experimental dissociation energies,[5,6] it is evident that the relative stabilities of the Nb_n (n=3–5) clusters could be correlated with their respective stabilities.

E. Dissociation energy (D_e), atomization energy (AE), ionization potential (IP), and electron affinity (EA) of Nb_4 and Nb_5

Armentrout and co-workers[5,6] have measured the IP and D_e of Nb_4 and Nb_5 clusters through a CID technique. The calculated and the experimental values of these quantities are compared in Table X. The PES of Nb_4^- and Nb_5^- have yielded the vertical EA (Ref. 3) of Nb_4 (1.15 eV) and Nb_5 (1.65 eV).

a. D_e of Nb_4. The dissociation energy of Nb_4 is computed at the MRSDCI level from reaction (1),

$$Nb_4\ (^1A',C_s)\rightarrow Nb_3\ (^2B_1)+Nb\ (^6D). \quad (1)$$

Since the ground state of Nb_3 at the MRSDCI+Q level is $^2A_1$, the D_e of Nb_4 at the MRSDCI+Q level is calculated as follows:

$$Nb_4\ (^1A',C_s)\rightarrow Nb_3\ (^2A_1)+Nb\ (^6D). \quad (2)$$

The calculations are carried out in a stepwise manner. Initially the dissociation energy (D_e') is calculated for the following supermolecular system:

$$Nb_4\ (^5A',C_s)\rightarrow Nb_3\ (^2A_1)+Nb\ (^6D). \quad (3)$$

The D_e' for reaction (3) was computed through a supermolecular approach by placing the apex Nb atom of the pyramid (C_s) structure of Nb_4 at 10 Å separation from the base atoms. The optimized structure of Nb_3 ($^2A_1$) at the CASMCSCF/MRSDCI level[21] was used for the triangular base structure to compute the energy of the supermolecular system. The energy difference between the $^5A'$ state of Nb_4 and the supermolecular $^5A'$ state gives the value of D_e' (MRSDCI, 4.79 eV, MRSDCI+Q, 4.99 eV). The actual D_e values of Nb_4 are then calculated at the MRSDCI and MRSDCI+Q levels by the use of reactions (1) and (2) and by the following adjustments of energies with respect to the ground states of Nb_3 and Nb_4:

$$D_e\ (\mathrm{MRSDCI})=D_e'-\Delta E\ (^2A_1,Nb_3)+\Delta E\ (^5A',Nb_4),$$

$$D_e\ (\mathrm{MRSDCI+Q})=D_e'+\Delta E\ (^5A',Nb_4).$$

Thus the calculated D_e values at the MRSDCI and MRSDCI+Q levels are 6.01 and 6.79 eV, respectively, in agreement with the experimental value quite well[5,6] (Table X).

The D_e of Nb_4 at the DFT/B3LYP level has been computed directly from reaction (1) using $(6s6p5d1f//6s4p4d1f)$ and $(6s6p5d1f1g//6s4p4d1f1g)$ basis sets. The D_e value is calculated as $D_e(Nb_4)=E(Nb_4,{}^1A')-E(Nb_3,{}^2B_1)-E(Nb,{}^6D)$. The D_e values thus calculated using the two basis sets (6.07 eV and 6.10 eV, Table IX) are consistent with the MRSDCI and MRSDCI+Q results and experiment.[5,6]

b. D_e of Nb_5. The dissociation energy of Nb_5 at the MRSDCI and MRSDCI+Q levels is computed in a stepwise manner as follows:

$$Nb_5\ (^2A_2,\mathrm{DTB})\rightarrow Nb_4\ (^1A')+Nb\ (^6D). \quad (4)$$

Initially the dissociation energy (D_e'') is calculated for the following system:

$$Nb_5\ (^6B_1,\mathrm{DTP})\rightarrow Nb_4\ (^1A_g,D_{2h})+Nb\ (^6D). \quad (5)$$

The D_e'' for the reaction (5) was calculated as supermolecular approach by placing the apex Nb atom of the DTP structure at 10 Å separation from the four Nb atoms of the base. The optimized geometry of the ^1A_g state (Table I) of Nb_4 was used to compute the energy of the supermolecular system. The energy difference between the $^6B_1$ state and the supermolecular $^6B_1$ state gives the value of D_e'' (MRSDCI, 4.68 eV, MRSDCI+Q, 5.04 eV). The actual D_e for reaction (4) is then calculated by the adjustments of energies with respect to the ground states of Nb_4 ($^1A',C_s$) and Nb_5 ($^2A_2$,DTB) [$D_e=D_e''+\Delta E\ (^6B_1,Nb_5)-\Delta E\ (^1A_g,Nb_4)$]. The D_e of Nb_5, thus calculated at the MRSDCI (5.58 eV) and MRSDCI+Q (6.25 eV) levels, agree with experiment[5,6] very well (Table X).

The D_e of Nb_5 at the DFT/B3LYP level has been computed directly by the use of the $(6s6p5d1f//6s4p4d1f)$ and $(6s6p5d1f1g//6s4p4d1f1g)$ basis sets as follows:

$$Nb_5\ (^2B_1,\mathrm{DTB})\rightarrow Nb_4\ (^1A')+Nb\ (^6D). \quad (6)$$

The D_e value is calculated as $D_e(Nb_5)=E(Nb_5,{}^2B_1)-E(Nb_4,{}^1A')-E(Nb,{}^6D)$. The D_e value thus calculated using both the basis sets (5.51 eV and 5.53 eV, Table IX) is consistent with the MRSDCI and MRSDCI+Q results and experiment.[5,6]

The AEs of Nb_4 and Nb_5 have been calculated from the stepwise D_e values of Nb_n clusters at the MRSDCI and MRSDCI+Q levels. Balasubramanian and Zhu[38] have calculated the D_e of Nb_2 to be 3.95 and 4.28 eV, respectively, at the MRSDCI and MRSDCI+Q levels. In our previous paper, we have calculated the D_e of Nb_3 at the MRSDCI (4.76 eV) and MRSDCI+Q (4.46 eV) levels. Combining these results, the AE/atom of Nb_4 comes out to be 3.68 and 3.88 eV/atom, respectively, at the MRSDCI and MRSDCI+Q levels. The AE/atom of Nb_5 could be similarly calculated using the stepwise D_e values of Nb_2, Nb_3, Nb_4, and Nb_5. The values thus computed are 4.06 and 4.36 eV/atom, respectively, at the MRSDCI and MRSDCI+Q levels. The calculated AE/atom of Nb_4 and Nb_5 clusters at the DFT/B3LYP level are 4.32 and 4.56 eV, respectively. All these results are in good agreement with the experimental AE/atom values of Nb_4 and Nb_5, obtained from the experimental D_e values[5,6] (Table X) of the Nb_n clusters.

c. EA of Nb_4 and Nb_5. The EA of Nb_4 has been calculated as the adiabatic energy difference between the optimized geometries of the ground states of Nb_4 and Nb_4^-. The DFT/B3LYP level of calculation used the $(6s6p5d1f//6s6p4d1f)$ and $(6s6p5d1f1g//6s6p4d1f1g)$ basis sets and the energy separation was calculated between the $^1A'$ and the $^2A'$ electronic states of Nb_4 and Nb_4^- for the calculation of EA. The EA of Nb_4 was calculated at the MRSDCI and MRSDCI+Q levels using the $(5s5p4d1f//5s3p2d1f)$ basis set. Higher-order basis set (cf. DFT/B3LYP calculation) could not be used, as the number of configurations in the CI calculation becomes enormously high. The energy difference between the $^1A'$ (Nb_4) and $^2B_{3g}$ (Nb_4^-) electronic states was calculated at these two levels to estimate the EA of Nb_4. Considering the adiabatic nature of the calculated EA, the calculated results (Table X) are in agreement with experiment[3] (1.15 eV). The MRSDCI+Q method predicts a slightly higher value (1.42 eV), but considering the uncertainty in the measured value of EA from the PES, this calculated value is also quite accurate.

The EA of Nb_5 was calculated at the DFT/B3LYP level using the energy difference of the ground states of Nb_5 ($^2A_2$) and Nb_5^- ($^1A_1$). Both the $(6s6p5d1f//6s6p4d1f)$ and $(6s6p5d1f1g//6s6p4d1f1g)$ basis sets were employed to calculate EA at this level. The calculated value (1.31 eV) (Table X) is somewhat lower than the experiment[3] (1.65 eV). However, it is well recognized that the computation of the adiabatic EAs of these species is extremely difficult.

The calculation of the EA of Nb_5 could not be carried out in a straightforward way at the MRSDCI and MRSDCI+Q levels due to a large number of configurations. For accurate calculations, at least 0.02 cutoffs of configurations are needed even with the use of the $(5s5p4d//5s3p2d)$ basis set, and the total configuration becomes enormously high. Consequently, the EA of Nb_5 was computed using the following thermodynamic cycle:

$$\mathrm{EA}\ (\mathrm{Nb_5}) = D_e^{\mathrm{I}}\ (\mathrm{Nb_5^-}) - D_e\ (\mathrm{Nb_5}) + \mathrm{EA}\ (\mathrm{Nb_4}). \quad \text{(I)}$$

$D_e^{\mathrm{I}}(\mathrm{Nb_5^-})$ involves the dissociation energy of Nb_5^- for the reaction $Nb_5^-\ (^3B_1,\mathrm{DTB}) \rightarrow Nb_4^-\ (^2B_{2g}) + Nb\ (^6D)$. The quantities $D_e(\mathrm{Nb_5})$ and $\mathrm{EA}(\mathrm{Nb_4})$ have already been calculated (Table X). The $D_e^{\mathrm{I}}(\mathrm{Nb_5^-})$ cannot be calculated in a straightforward way through a supermolecular approach, as Nb_5^- dissociates as Nb_4 and Nb^- at the MRSDCI level. Thus the D_e^{I} value is calculated in a stepwise manner.

Initially the dissociation energy D_e^{II} is calculated for the following reaction:

$$\mathrm{Nb_5^-}\ (^3B_1,\mathrm{DTP}) \rightarrow \mathrm{Nb_4}\ (^5B_{1g}) + \mathrm{Nb^-}\ (\mathrm{quintet}). \quad (7)$$

The calculation is done through a supermolecular approach by placing the apex Nb atom of a tetragonal pyramid structure at 10 Å separations from four base Nb atoms. The $^5B_{1g}(D_{2h})$ structure of Nb_4 (Table I) is used for the base structure. The dissociation energy D_e^{II} is then calculated by taking the energy difference between the $^3B_1$ (DTP) state of Nb_5^- and the $^3B_1$ state of supermolecule. The adjustment of energy separations with respect to the ground states of $Nb_5^-\ (^3B_1,\mathrm{DTB})$ and $Nb_4^-\ (^1A')$ gives the dissociation energy (D_e^{I}) for reaction (8a) from relation (8b):

$$\mathrm{Nb_5^-}\ (^3B_1,\mathrm{DTB}) \rightarrow \mathrm{Nb_4}\ (^1A') + \mathrm{Nb^-}\ (\mathrm{quintet}), \quad \text{(8a)}$$

$$D_e^{\mathrm{III}} = D_e^{\mathrm{II}} + \Delta E\ (^3B_1,\mathrm{DTP}) - \Delta E\ (^5B_{1g}). \quad \text{(8b)}$$

Since the ground state of Nb_5 at the MRSDCI+Q level is $^1A_1$, the energy adjustments are made with respect to this state during D_e^{III} calculation at this level. The calculated D_e^{III} at the MRSDCI (6.77 eV) and MRSDCI+Q (7.13 eV) levels are used in the energy cycle (8c) to calculate the dissociation energy $D_e^{\mathrm{I}}(\mathrm{Nb_5^-})$,

$$D_e^{\mathrm{I}}\ (\mathrm{Nb_5^-}) = D_e^{\mathrm{III}} + \mathrm{EA}\ (\mathrm{Nb_4}) - \mathrm{EA}\ (\mathrm{Nb}). \quad \text{(8c)}$$

We have calculated the electron affinity of Nb atom at the DFT/B3LYP level to be 2.14 eV using the $(6s6p5d1f//6s6p4d1f)$ basis set. Since all the parameters on the right side of Eq. (8c) are now known, the calculation of $D_e^{\mathrm{I}}(\mathrm{Nb_5^-})$ at the MRSDCI (5.87 eV) and MRSDCI+Q (6.41 eV) is quite straightforward. We have checked these numbers against our DFT/B3LYP (6.01 eV), using the $(6s6p5d1f//6s6p4d1f$ basis set) and the previous LSD (Ref. 20) (6.32 eV) results. Our calculated $D_e^{\mathrm{I}}(\mathrm{Nb_5^-})$ is quite satisfactory with respect to these values. The electron affinity of Nb_5 can now be calculated from relation (8b). The calculated EA of Nb_5 at the MRSDCI (1.54 eV) and MRSDCI+Q (1.58 eV) levels are in excellent agreement with the experiment[3] (1.65 eV, Table X).

d. IP of Nb_4 and Nb_5. The IPs of Nb_4 and Nb_5 at the DFT/B3LYP level have been calculated by taking the energy difference of the ground states of cationic and neutral clusters. The calculations have been carried out using both the $(6s6p5d1f//6s4p4d1f)$ and $(6s6p5d1f1g//6s4p4d1f1g)$ basis sets. In the case of Nb_4 IP calculation, the energy difference was taken between the $^1A'\ (\mathrm{Nb_4})$ and $^2A'\ (\mathrm{Nb_4^+})$ electronic states while for the IP calculation of Nb_5 the energy difference was calculated between the $^2B_1\ (\mathrm{Nb_5},\mathrm{DTB})$ and $^3A_1\ (\mathrm{Nb_5^+},\mathrm{DTP})$ electronic states. The calculated IP values of Nb_4 (5.43 eV) and Nb_5 (5.22 eV) are in very good agreement with the experiment[5,39] (Table X). It is to be noted further from Table X that the use of g function in the basis set does not change the IP significantly.

The calculation of the IP values of Nb_4 and Nb_5 at the MRSDCI and MRSDCI+Q levels turned out to be more challenging than the DFT/B3LYP technique. This way of calculating the IP needs a bigger basis set. The minimum basis set for this purpose should use an extra d and a f function together with sp diffuse functions: $[(6s6p4d1f//6s4p3d1f)$ type]. The MRSDCI calculation using such a basis set is intractable even for Nb_4^+. The use of lower order basis sets of the type $(5s5p4d1f//5s3p2d1f)$ and $(6s6p4d//6s4p3d)$ does not produce any reliable results (Table X). Thus the IP calculations at the MRSDCI and MRSDCI+Q levels have been carried out using a thermodynamic cycle. The following thermodynamic cycle relation is used for the calculations of IPs:

$$\mathrm{IP}(\mathrm{Nb}_n) = \mathrm{IP}(\mathrm{Nb}_{n-1}) - D_e\ (\mathrm{Nb}_{n-1}^+ - \mathrm{Nb}) + D_e\ (\mathrm{Nb}_{n-1} - \mathrm{Nb}) \quad (n = 4,5). \quad (9)$$

Thus the calculation of IP values needs accurate measures of the dissociation energies of Nb_n and Nb_n^+. Since our computed D_e values Nb_4 and Nb_5 are quite accurate (Table X), and we have previously calculated the D_e values[31] of Nb_4^+ (6.70 eV) and Nb_5^+ (6.08 eV), we can use these results to compute the IP. Although these values are within the range of the experimental data, they are not precise enough for the IP calculations through Eq. (9). Thus we have first recalculated the D_e values of Nb_4^+ and Nb_5^+ using larger CI and basis set calculations to maintain consistency. The following dissociation reactions are used for the calculation of D_e values of Nb_4^+ and Nb_5^+, respectively.

$$\mathrm{Nb_4^+}\ (^2A',C_s) \rightarrow \mathrm{Nb_3^+}\ (^3A_2) + \mathrm{Nb}\ (^6D), \quad (10)$$

$$\mathrm{Nb_5^+}\ (^1A',\mathrm{DECT}) \rightarrow \mathrm{Nb_4^+}\ (^2A') + \mathrm{Nb}\ (^6D). \quad (11)$$

The same supermolecular approach as described in our previous paper[31] has been used for the calculation of the D_e values. In the case of Nb_5^+, the only difference is that we have used much bigger CI calculations. In the case of Nb_4^+ we have calculated the D_e value in a stepwise manner. The D_e' value is first computed for the following dissociation process in a supermolecular scheme:

$$\mathrm{Nb_4^+}\ (^6A',C_s) \rightarrow \mathrm{Nb_3^+}\ (^3A_2) + \mathrm{Nb}\ (^6D). \quad (12)$$

This step is different from our previous approach where we have initially dissociated the $^4A'\ (C_s)$ state of Nb_4^+ instead of the $^6A'$ state. The measurement of D_e' is done in the same supermolecular approach as described in our previous

paper.[31] The actual D_e is obtained through adjustment of the ground state energies of Nb_3^+ and Nb_4^+ from the following relation:

$$D_e = D_e' + \Delta E\ (^6A') - \Delta E\ (^3A_2). \quad (13)$$

Our calculated D_e values of Nb_4^+ (MRDCI, 6.01 eV; MRSDCI+Q, 6.64 eV) and Nb_5^+ (MRSDCI, 5.43 eV; MRSDCI+Q, 5.76 eV) are in very good agreement with the experiment[5,6] (Table X). The IP values could now be calculated from relation (9), as all the parameters needed have been determined with sufficient accuracy (Table X). The calculated IP values of Nb_4 (MRSDCI, 5.60 eV; MRSDCI+Q, 5.76 eV) and Nb_4 (MRSDCI, 5.39 eV; MRSDCI+Q, 5.71 eV) are in excellent agreement with the experiment.[5,39]

F. Assignment of the photoelectron spectrum of Nb_4^- and Nb_5^-

Kietzmann and co-workers[3] have measured the PES of Nb_4^- and Nb_5^- through a laser vaporization technique. The spectra yielded the EAs of these two clusters and the positions of the various low-lying electronic states of the neutral Nb_n ($n=4,5$). Since the spectrum was not vibrationally resolved, the excitation energies measured from the spectra would be vertical in nature. Fournier, Pang, and Chen[20] have used a scaling technique for the virtual orbital energies of Nb_n^- ($n=4,5$) to match the locations of the excited states in the spectra. Their scaling method was quite successful in predicting the excitation energies of the various excited states of the Nb_n ($n=4,5$) clusters observed in the spectrum. But this technique gives no information on the nature of the excited states. Our present calculations provide the geometries, symmetries, and the energy separations of the ground and low-lying exited states of Nb_4 and Nb_5. Since our calculations are based on the optimized geometries of the respective states, the excitation energies of the electronic states are all adiabatic. The assignments presented here are based upon our MRSDCI results on Nb_4 (Table I) and Nb_5 (Table III), as the MRSDCI method gives the most reliable energy separations of the various electronic states and predicts the EAs of the Nb_n ($n=4,5$) clusters very accurately (Table X).

The PES (Ref. 3) of Nb_4^- has four intense peaks at 1.15, 1.6, 2.0, and 3.0 eV, respectively (Table I). The first intense peak corresponds to the electron affinity of Nb_4. Our MRSDCI results assign the formation of this peak from the $^2B_{3g}$ state of Nb_4^- (Table VI) to the ground state of Nb_4 ($^1A'$) through electron detachment. The feasibility of this process has already been discussed in Sec. III C a. The calculation of the EA of Nb_4 (Sec. III E b) would further justify this assignment. The first low-lying excited state is 0.45 eV above the ground state. On the basis of the MRSDCI ΔE (Table I), the ^1A_g state ($\Delta E=0.67$ eV) is a possible candidate for this state. The third intense peak in the PES is at 0.85 eV relative to the ground state of Nb_4. The possible candidate for this peak is $^3B_{3u}$ ($\Delta E=0.82$ eV, Table I). The fourth intense peak is at an energy separation of 1.75 eV from the ground state and according to our MRSDCI results, the $^5A'$ ($\Delta E=1.44$ eV) and $^5B_{1g}$ ($\Delta E=1.40$ eV) are suitable candidates for this state. This peak is actually broad at 1.85 eV, where we find a cluster of electronic states. According to our MRSDCI results the $^5A''$ ($\Delta E=1.84$ eV), $^3B_{1g}$ ($\Delta E=1.88$ eV), and $^5B_{3g}$ ($\Delta E=1.88$ eV) states are likely candidates for this peak.

There is a weak peak at 2.5 eV in the PES, which suggests a state at 1.35 eV from the ground state. According to our MRSDCI calculation, four electronic states of Nb_4 [$^1A''$ ($\Delta E=1.08$ eV), $^3B_{2u}$ ($\Delta E=1.12$ eV), $^1B_{2g}$ ($\Delta E=1.22$ eV), and $^3A'$ ($\Delta E=1.28$ eV)] lie in this region. Finally, there is another peak at the higher energy range (3.4 eV peak) in the PES, which corresponds to an electronic state with an energy separation of 2.25 eV. Three electronic states, viz., $^1B_{1g}$ ($\Delta E=1.99$ eV), $^1B_{2u}$ ($\Delta E=2.23$ eV), and $^3A''$ ($\Delta E=2.24$ eV) are probable candidates for this peak.

The PES (Ref. 3) of Nb_5^- has three intense peaks at 1.65, 2.4, and 3.2 eV, respectively (Table III). The first intense peak corresponds to the electron affinity of Nb_5. Our MRSDCI results assign the formation of this peak to originate from the $^1A_1$ (DTB) state of Nb_5^- (Table VIII) to the ground state of Nb_5 ($^2A_2$,DTB) through electron detachment. We have already discussed in Sec. III C b that out of the two competing ground states for Nb_5^- ($^3B_1$ and $^1A_1$, Table VIII), the formation of the $^2A_2$ state of Nb_5 is more feasible from the $^1A_1$ state of Nb_5^-. The calculation of the EA of Nb_5 (Sec. III E c) would further justify this assignment. The first low-lying excited state is 0.35 eV from the ground state and this appears as a shoulder on the first intense peak in the PES (at 2.0 eV region). According to the MRSDCI ΔE values (Table III), both the $^4A_1$ ($\Delta E=0.41$ eV) and $^4B_1$ ($\Delta E=0.43$ eV) states of the DTB structure are the possible candidates for this state. Apart from these two states, the $^2A''$ state of the DECT structure is also a probable candidate. Although the MRSDCI results ($\Delta E=0.08$ eV) suggest that this may be a potential candidate for the ground state, the MRSDCI+Q results ($\Delta E=0.31$ eV) place it around the shoulder peak (2.0 eV region) of the PES. The second intense peak in the PES is at 0.75 eV energy from the ground state of Nb_5. The possible candidates for this peak are $^4A_1$ (DTP,$\Delta E=0.73$ eV), $^2A_1$ (DTB,$\Delta E=0.87$ eV), and $^6B_2$ (DTB,$\Delta E=0.91$ eV) (Table III). However, $^4A_1$ (DTP) should be considered a more probable candidate for this peak.

The third intense peak of the PES of Nb_5^- is at 3.2 eV[3] (energy separation of 1.55 eV) with a shoulder at around 2.9 eV (separation 1.25 eV). The MRSDCI results (Table III) assign the $^6A_1$ (DTB,$\Delta E=1.20$ eV) and $^6A_2$ (DTP,$\Delta E=1.25$ eV) states as candidates for the shoulder peak at 2.9 eV. On the basis of our MRSDCI results, only $^6B_1$ state of the DTP structure ($\Delta E=1.57$ eV) could be assigned for the intense peak at 3.2 eV. Apart from these peaks in PES of Nb_5^-, there lies a weak peak at 3.4 eV[3] (energy separation of 1.75 eV). The MRSDCI results in Table III suggest that the $^6A''$ (DECT,$\Delta E=1.78$ eV), $^4B_2$ (DTP,$\Delta E=1.69$ eV), and the $^2B_2$ (DTP,$\Delta E=1.74$ eV) states are candidates for this peak. It is to be noted that the excitation energies of the observed PES are vertical in nature. In view of the uncertainty in the measurement of peak positions, our assignment of the spectra at the MRSDCI level is quite consistent.

G. The nature of bonding in Nb_n and Nb_n^- (n=4,5): Electronic configurations, orbital composition, and Mulliken populations

The leading configurations of the low-lying electronic states of Nb_n and Nb_n^- (n=4,5) at the CASMCSCF/MRSDCI level reveal their multireference characters. Most of the electronic states of these clusters have less than 80% contributions from the leading configurations. However, for most of the electronic states the dominant configurations at the CASMCSCF/MRSDCI level are the same as those at the DFT/B3LYP level. Thus the calculated geometries and the energy separations at both the levels are similar. The correlation effects originating due to multireference nature of the wave functions in the CASMCSCF/MRSDCI calculations are different from those of the DFT/B3LYP level. Thus, in most of the cases, some differences are observed in the geometric and energetic features of different electronic states at these two levels. In few cases this difference is quite appreciable. One such case is the difference in the geometry and the observed energy separation between the two Jahn-Teller components, $^1A'$ and $^1A''$ states of Nb_4 at the CASMCSCF/MRSDCI and DFT/B3LYP levels. The origin of these differences has been attributed to the multireference characters of these two states and has already been discussed in details (Sec. III B). The other interesting differences, which are originating due to multireference nature of these electronic states, have been discussed in Secs. III A and III C.

a. Nb_4 and Nb_4^-. The leading electronic configuration of the $^1A'$ ground state of Nb_4 (Table I) is $1a'^2\cdots 17a'^2 1a''^2\cdots 9a''^2$ (69%). The higher energy Jahn-Teller component of this electronic state ($^1A''$) is actually formed through excitation of the electron from the doubly occupied a' orbital of the $^1A'$ ground state to the lowest vacant a'' orbital $[1a'^2\cdots 16a'^2 17a'^1 1a''^2\cdots \times 9a''^2 10a''^1$ (67%)]. The first low-lying excited state (^1A_g) has also a closed shell structure and has the $1a_g^2\cdots 7a_g^2 1b_{1u}^2\cdots 3b_{1u}^2 1b_{2u}^2\cdots 4b_{2u}^2 1b_{3g}^2 1b_{3u}^2\cdots 5b_{3u}^2 1b_{2g}^2 \times 2b_{2g}^2 1b_{1g}^2\cdots 3b_{1g}^2 1a_u^2$ (43%) dominant configuration. It has already been discussed in Sec. III C that the ground state $^3B_{3g}$ of Nb_4^- generates the $^1A'$ state through electron detachment. Although the ^1A_g state is highly stabilized through electron correlation effects (Sec. III A), the electron detachment of the $^3B_{3g}$ state of Nb_4^- does not lead to the ^1A_g state of Nb_4. Thus the $^1A'$ state is stabilized over the ^1A_g state by electron correlation effects.

The next low-lying electronic state of Nb_4 ($^3B_{3u}$) is formed by the excitation of the electron of the doubly occupied a_u orbital of the ^1A_g state to the vacant b_{3g} orbital $[1a_g^2\cdots 7a_g^2\ 1b_{1u}^2\cdots 3b_{1u}^2 1b_{2u}^2\cdots 4b_{2u}^2 1b_{3g}^2 2b_{3g}^1 1b_{3u}^2\cdots \times 5b_{3u}^2 1b_{2g}^2 2b_{2g}^2 1b_{1g}^2\cdots 3b_{1g}^2 1a_u^1$ (66%)]. Thus $^3B_{3u}$ is slightly higher (ΔE=0.82 eV) than the ^1A_g state. The $^2B_{2u}$ is the excited state of $^3B_{3u}$ (ΔE=1.12 eV) and is formed by a double excitation of electrons from the a_g and b_{2u} orbitals to the a_u and b_{3g} orbitals $[1a_g^2\cdots 6a_g^2 7a_g^1 1b_{1u}^2 \cdots 3b_{1u}^2 1b_{2u}^2\cdots 3b_{2u}^2 4b_{2u}^1 1b_{3g}^2 2b_{3g}^2 1b_{3u}^2\cdots 5b_{3u}^2 1b_{2g}^2 2b_{2g}^2 \times 1b_{1g}^2\cdots 3b_{1g}^2 1a_u^2$ (58%)]. The $^1B_{2g}$ excited state is formed from the $^3B_{3u}$ state by excitation of an electron of the doubly occupied b_{1g} orbital to the singly occupied a_u orbital $[1a_g^2\cdots 7a_g^2 1b_{1u}^2\cdots 3b_{1u}^2 1b_{2u}^2\cdots 4b_{2u}^2 1b_{3g}^2 2b_{3g}^1 1b_{3u}^2\cdots 5b_{3u}^2 \times 1b_{2g}^2 2b_{2g}^2 1b_{1g}^2\cdots 3b_{1g}^1 1a_u^2$ (58%)], while the $^1B_{2u}$ state is formed from the $^3B_{2u}$ state by a double excitation of electrons from the b_{1u} and b_{3g} orbitals to the a_g and b_{2u} orbitals $[1a_g^2\cdots 7a_g^2 1b_{1u}^2 2b_{1u}^2 3b_{1u}^1 1b_{2u}^2\cdots 3b_{2u}^2 4b_{2u}^2 1b_{3g}^2 2b_{3g}^1 1b_{3u}^2\cdots \times 5b_{3u}^2 1b_{2g}^2 2b_{2g}^2 1b_{1g}^2\cdots 3b_{1g}^2 1a_u^2$ (41%)].

The leading configuration of the ground state of Nb_4^- ($^2B_{3g}$) is $1a_g^2\cdots 7a_g^2 1b_{1u}^2\cdots 3b_{1u}^2 1b_{2u}^2\cdots 4b_{2u}^2 1b_{3g}^2 \times 2b_{3g}^1 1b_{3u}^2\cdots 5b_{3u}^2 1b_{2g}^2 2b_{2g}^2 1b_{1g}^2\cdots 3b_{1g}^2 1a_u^2$ (73%). The first low-lying excited state ($^4B_{1u}$) is formed from the $^2B_{2g}$ ground state by the excitation of the electron of the doubly occupied a_g orbital to the vacant b_{2u} orbital $[1a_g^2\cdots 6a_g^2 7a_g^1 1b_{1u}^2\cdots 3b_{1u}^2 1b_{2u}^2\cdots 4b_{2u}^2 5b_{2u}^1 1b_{3g}^2 2b_{3g}^1 \times 1b_{3u}^2\cdots 5b_{3u}^2 1b_{2g}^2 2b_{2g}^2 1b_{1g}^2\cdots 3b_{1g}^2 1a_u^2$ (76%)]. The $^2A'$ and $^2A''$ states of the C_s structure are higher energy states and are nearly degenerate. Both the states are highly multireference in character [$^2A'$: $45\%|1a'^2\cdots 16a'^2 17a'^1 \times 1a''^2\cdots 10a''^2\rangle + 16\%|1a'^2\cdots 16a'^2 17a'^1 1a''^2\cdots 9a''^2 \times 10a''^1 11a''^1\rangle + \cdots$; $^2A''$: $53\%|1a'^2\cdots 17a'^2 1a''^2\cdots \times 9a''^2 10a''^1\rangle + 19\%|1a'^2\cdots 16a'1a''^2\cdots 10a''^2 11a''^1\rangle + \cdots$]. The two states are nearly degenerate due to the counterbalancing electron correlation effects from the two leading configurations contributing to these states. The relative stabilities of all the low-lying electronic states of Nb_4 and Nb_4^- could be similarly explained from the properties of their leading electronic configurations.

b. Nb_5 and Nb_5^-. The leading configuration of the ground state of the Nb_5 cluster ($^2A_2$, DTE, Table III) is $1a_1^2\cdots 13a_1^2 1b_2^2\cdots 9b_2^2 1b_1^2\cdots 7b_1^2 1a_2^2\cdots 3a_2^2 4a_2^1$ (66%). The first two low-lying excited states $^4A_1$ (DTB) $[1a_1^2\cdots \times 13a_1^2 1b_2^2\cdots 8b_2^2 9b_2^1 1b12\cdots 7b_1^2 8b_1^1 1a_2^2\cdots 3a_2^2 4a_2^1$ (67%)] and $^4B_1$ (DTB) $[1a_1^2\cdots 13a_1^2 14a_1^1 1b_2^2\cdots 8b_2^2 9b_2^1 1b_1^2\cdots \times 7b_1^2 1a_2^2\cdots 3a_2^2 4a_2^1$ (66%)] are formed from the $^2A_2$ (DTB) ground state through the excitation of the $9b_2$ electron into the vacant $8b_1$ orbital ($^4A_1$) or the $14a_1$ ($^4B_1$) orbital. Thus these two low-lying states are almost degenerate. The next higher electronic state $^2A_1$ (DTB) is also an excited state of the $^2A_2$ ground state. This state is formed from the excitation of the doubly occupied $13a_1$ orbital of the ground state into the $4a_2$ singly occupied orbital $[1a_1^2\cdots 12a_1^2 13a_1^1 1b_2^2\cdots \times 9b_2^2 1b_1^2\cdots 7b_1^2 1a_2^2\cdots 4a_2^2$ (69%)].

The $^4A_1$ and $^4B_2$ electronic states of the DTP structure are Jahn-Teller components with the $^4B_2$ state being higher (ΔE=1.69 eV, Table III). The leading configuration of the $^4B_2$ state is $1a_1^2\cdots 13a_1^2 14a_1^1 1b_2^2\cdots 8b_2^2 1b_1^2 \cdots 7b_1^2 8b_1^1 1a_2^2\cdots 3a_2^2 4a_2^1$(64%). It is formed from the $^4A_1$ state $[1a_1^2\cdots 13a_1^2 1b_2^2\cdots 8b_2^2 9b_2^1 1b12\cdots 7b_1^2 8b_1^1 1a_2^2 \cdots 3a_2^2 4a_2^1$ (66%)] by promoting a $9b_2$ electron into the vacant $14a_1$ orbital. The lowest energy electronic state of the DECT structure is $^2A''$ [ΔE=0.08 eV,$1a'^2\cdots 21a'^2 1a''^2\cdots \times 11a''^2 12a''^1$ (69%)]. The $^2A'$ electronic state [ΔE=1.06 eV,$1a'^2\cdots 20a'^2 21a'^1 1a''^2\cdots 12a''^2$ (67%)] is formed from the $^2A''$ state through excitation of the doubly occupied a' orbital into the singly occupied $12a''$ orbital.

The Nb_5^- cluster has two nearly degenerate ground states, $^3B_1$ and $^1A_1$ (Table VIII) of the DTB structure. We have discussed in Sec. III C that the $^1A_1$ state is the more favored ground state at higher levels. The first low-lying $^1B_1$ excited state (DTB) has a similar leading configuration $[1a_1^2\cdots 14a_1^2 1b_2^2\cdots 8b_2^2 9b_2^1 1b_1^2\cdots 7b_1^2 1a_2^2\cdots 3a_2^2 4a_2^1$ (45%)]

to the $^3B_1$ state. The only difference is that the $^3B_1$ state has more α electrons in the b_2 and a_2 orbitals ($9b_2^1 4a_2^1$). Thus the $^3B_1$ state acquires enhanced stability owing to maximization of spin exchange energy (Hund's rule). The $^3A_2$ ($\Delta E = 0.19$ eV) and the $^3B_2$ ($\Delta E = 0.19$ eV) states are excited states. The $^3A_2$ (DTB) state $[1a_1^2 \cdots 13a_1^2 14a_1^1 1b_2^2 \cdots 9b_2^2 1b_1^2 \cdots 7b_1^2 1a_2^2 \cdots 3a_2^2 4a_2^1 (36\%)]$ and the $^3B_2$ state (DTB) $[1a_1^2 \cdots 13a_1^2 14a_1^1 1b_2^2 \cdots 8b_2^2 9b_2^1 1b_1^2 \cdots 7b_1^2 1a_2^2 \cdots 4a_2^2 (72\%)]$ are formed from the $^3B_1$ state by the excitation of electrons of the doubly occupied $14a_1$ orbital into singly occupied $9b_2$ ($^3A_2$) or $4a_2$ ($^3B_2$) orbitals. In fact, the $^3B_1$ and $^3A_2$ states are the results of Jahn-Teller distortion, and the $^3A_2$ state is the higher energy component. The energy ordering of the rest of the electronic states of Nb_5 and Nb_5^- clusters could be similarly explained from their leading electronic configurations.

c. Orbital compositions. The compositions of the natural orbitals in the MRSDCI wave function of the ground $^1A'$ (C_s) and the first excited ^1A_g (D_{2h}) electronic states of Nb_4 are qualitatively represented below. Only a few representative orbitals are expanded in this manner. Figure 2 shows the pictures of a few selected active space orbitals of these electronic states presented below.

(1) Nb_4 ($^1A'$),

$$\psi(15a') = (Nb_1 + Nb_2 - Nb_3)(5s) - (Nb_1 + Nb_2 + Nb_3) \times (5p_y) + (Nb_2 + Nb_2 + Nb_4)(5p_x + 4d_x2_{+y}2_{-2z}2) + (Nb_1 - Nb_2)(5p_z) - (Nb_1 + Nb_2 - Nb_4)(4d_{xy}) + (Nb_3)(4d_x2_{-y}2),$$

$$\psi(16a') = -(Nb_1 + Nb_2)(5s + 4d_x2_{+y}2_{-2z}2) + (Nb_1 - Nb_2)(5p_z - 4d_{xz} + 4d_{yz}) - (Nb_4) \times (4d_x2_{+y}2_{-2z}2),$$

$$\psi(17a') = -(Nb_1 + Nb_2 + Nb_3)(4d_x2_{+y}2_{-2z}2) - (Nb_1 - Nb_2)(4d_{xy}) + (Nb_1 - Nb_2)(4d_{xz} + 4d_{yz}) + (Nb_4)(5p_x),$$

$$\psi(7a'') = -(Nb_1 - Nb_2)(5s + 5p_x - 5p_y - 4d_x2_{+y}2_{-2z}2) - (Nb_1 + Nb_2)(5p_z) + (Nb_3 + Nb_4)(4d_{xz}) - Nb_3(4d_{yz}),$$

$$\psi(8a'') = (Nb_1 - Nb_2)(4d_x2_{+y}2_{-2z}2 + 4d_{xy}) - (Nb_3 - Nb_4)(4d_{xz} - 4d_{yz}) + (Nb_4)(5p_z),$$

$$\psi(9a'') = (Nb_1 + Nb_2)(5p_z) + (Nb_1 - Nb_2)(4d_{xy}) + (Nb_3)(4d_{xz}) + (Nb_3 - Nb_4)(4d_{yz}).$$

(2) Nb_4 (^1A_g),

$$\psi(6a_g) = -(Nb_1 - Nb_2)(5p_y) + (Nb_3 + Nb_4)(5s) - (Nb_3 - Nb_4)(5p_x) + (Nb_1 + Nb_2 - Nb_3 - Nb_4)(4d_x2_{-y}2),$$

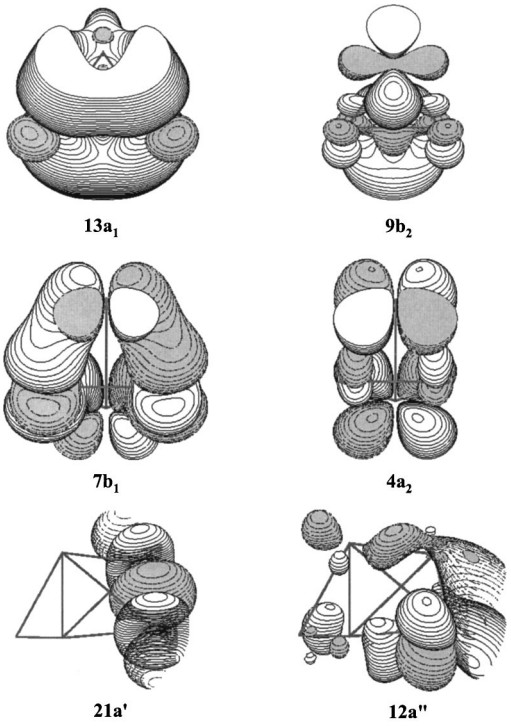

FIG. 3. The active space MOs of the ground ($^2A_2$,DTB) and the low-lying excited state ($^2A'', C_s$) of Nb_5. Only a few selected MOs of these two electronic states [$13a_1$, $9b_2$, $7b_1$, $4a_2$ ($^2A_2$), $21a'$, and $12a''$ ($^2A''$)], calculated at the CAMCSCF/MRSDCI level, are presented here. The pictures were originally drawn keeping z as the vertical axis. Each MO picture is then rotated to have better visualization.

$$\psi(7a_g) = (Nb_1 + Nb_2 + Nb_3 + Nb_4)(5p_z) + (Nb_1 - Nb_2) \times (4d_{yz}) + (Nb_3 - Nb_4)(4d_{xz}),$$

$$\psi(3b_{1u}) = (Nb_1 + Nb_2 + Nb_3 + Nb_4)(5s - 4d_x2_{+y}2_{-2z}2) - (Nb_3 - Nb_4)(5p_x),$$

$$\psi(4b_{2u}) = (Nb_1 - Nb_2)(5s + 4d_x2_{+y}2_{-2z}2) - (Nb_3 + Nb_4)(5p_y) - (Nb_3 - Nb_4)(4d_{xy}),$$

$$\psi(4b_{3u}) = (Nb_1 + Nb_2 - Nb_3 - Nb_4)(5p_x) + (Nb_1 - Nb_2) \times (4d_{xy}) - (Nb_3 - Nb_4)(5s + 4d_x2_{+y}2_{-2z}2),$$

$$\psi(2b_{2g}) = -(Nb_1 + Nb_2 - Nb_3 - Nb_4)(4d_{xz}) + (Nb_3 - Nb_4)(5p_z),$$

$$\psi(3b_{1g}) = -(Nb_1 + Nb_2)(5p_x) - (Nb_1 + Nb_2 + Nb_3 + Nb_4)(4d_{xy}) - (Nb_3 - Nb_4)(5p_y),$$

$$\psi(1a_u) = -(Nb_1 + Nb_2)(4d_{xz}) - (Nb_3 - Nb_4)(4d_{yz}).$$

As can be seen from above, considerable $5s$-$4d$ overlap is observed in most of the orbitals presented here except for the $1a_u$ orbital (^1A_g), which is composed of pure d orbitals. The orbital compositions further reveal that there are considerable p orbital mixings in most of the orbitals presented for the $^1A'$ and ^1A_g electronic states of Nb_4. The compositions thus indicate that apart from the σ orbital interaction, there is considerable π overlap between the Nb atoms in these orbit-

als. Thus it could be expected that there would be considerable *s* and *p* electron donation and back donation between the atoms to facilitate Nb-Nb bonding.

The natural orbital compositions of a few representative orbitals (at the MRSDCI level) of the $^2A_2$ (DTB) ground state and the low-lying $^2A''$ are shown below together with the pictures of $13a_1$, $9b_2$, $7b_1$, $4a_2$ ($^2A_2$), $21a'$, and $12a''$ in Fig. 3. These compositions also show a similar Nb-Nb bonding trend.

(3) Nb_5 (DTB, $^2A_2$),

$$\psi(12a_1) = -(Nb_1)(4d_x2_{-y}2) + (Nb_2+Nb_3)(5s) - (Nb_2-Nb_3)(5p_x) + (Nb_2+Nb_3+Nb_4+Nb_5)(4d_x2_{+y}2_{-2z}2) - (Nb_4-Nb_5)(4d_{yz}),$$

$$\psi(13a_1) = (Nb_1+Nb_2+Nb_3-Nb_4-Nb_5)(5s) - (Nb_1)\times(4d_x2_{-y}2) - (Nb_2+Nb_3)(4d_x2_{+y}2_{-2z}2) - (Nb_2-Nb_3-Nb_4+Nb_5)(4d_{yz}) - (Nb_4-Nb_5)(5p_y),$$

$$\psi(8b_2) = -(Nb_1+Nb_2+Nb_3+Nb_4+Nb_5)(5p_y) - (Nb_2-Nb_3)(4d_{xy}) + (Nb_4-Nb_5)(5s + 4d_x2_{+y}2_{-2z}2) + (Nb_4+Nb_5)(4d_{yz}),$$

$$\psi(9b_2) = (Nb_1-Nb_2-Nb_3)(5p_y) - (Nb_1+Nb_2+Nb_3)\times(4d_{yz}) - (Nb_4-Nb_5)(5s+4d_x2_{+y}2_{-2z}2) - (Nb_4+Nb_5)(4d_{yz}),$$

$$\psi(7b_1) = (Nb_1-Nb_4-Nb_5)(4d_{xz}) - (Nb_2-Nb_3)(5s + 4d_x2_{+y}2_{-2z}2) - (Nb_4-Nb_5)(4d_{xy}),$$

$$\psi(4a_2) = (Nb_1+Nb_2+Nb_3+Nb_4+Nb_5)(4d_{xy}) - (Nb_2 - Nb_3)(5p_y) + (Nb_4+Nb_5)(5p_x+4d_{xz}).$$

(4) Nb_5 (DECT, $^2A''$),

$$\psi(21a') = -(Nb_1+Nb_5)(5s+4d_x2_{+y}2_{-2z}2-4d_{xy}),$$

$$\psi(12a'') = -(Nb_1+Nb_2+Nb_3)(5p_z) - (Nb_2-Nb_3)(5s - 5p_y) + (Nb_4+Nb_5)(4d_{yz}) + (Nb_5)(4d_{xz}).$$

The orbital compositions seem to influence the relative stabilities of the various electronic states. It has already been found that the D_e values of Nb_n ($n=4,5$) clusters are quite high and are almost close to those of the Nb_n^+ ($n=4,5$) clusters (Table X). The $4d^45s^1$ ground state configuration of the Nb atom indicates that the principal bonding features of Nb_3 are governed by the *s*-*s* and *d*-*d* overlaps. This is supported by the orbital compositions of the Nb_4 and Nb_5 clusters, as discussed in this section. The 5*s* orbital has four radial nodes compared to one of the 4*d* orbitals. These characteristics of the 5*s* orbital, together with the relativistic mass-velocity effect,[40,41] allow it to penetrate the core more than the 4*d* orbital. The Mulliken populations reveal that the 5*s* and 4*d* orbitals involve substantial exchange of electrons with the 5*p* orbitals. In the case of the $^1A'$ electronic state of Nb_4, the total *s* and *d* orbital populations are 12.49 and 15.36, respectively. Considering the total population of 4*s* for all four atoms to be 8, the total 5*s* population of $^1A'$ is 4.49 (gain of electron 0.49*e*). The total 4*d* orbital population for all four Nb atoms is smaller (loss of 0.64*e*) than the total number of electrons (16). This suggests that the exchange of electron density with the 5*p* orbital results in Nb-Nb bonds that are not purely σ type. Similar conclusions could be deduced from the Mulliken population results on the ground state ($^2A_2$) of Nb_5. The penetration of the 5*s* orbital into the core leads to the possibility of substantial *d*-*d* overlap. The orbital compositions of Nb_4 and Nb_5 reveal that there is substantial π overlap of the 4*d* and 5*p* orbitals. These π overlaps facilitate the formation of multiple bonds between the Nb atoms and shortening of the Nb-Nb bonds. The average Nb-Nb bonding distances in the ground state of Nb_4 ($^1A'$) and Nb_5 ($^2A_2$) are 2.59 and 2.65 Å, respectively. When compared with the covalent radius of Nb atom (1.34 Å), these average bond lengths show that the Nb-Nb bonds are actually shortened, and they correlate well with the observed dissociation energy of Nb_4 and Nb_5.

The bonding analysis presented above clearly shows that there is considerable 5*p*-orbital participation in the formation of the Nb-Nb bonds apart from the 5*s*-4*d* mixings. The difference density plot of the $^1A'$ electronic state of Nb_4 and the $^2A_2$ (DTB) Nb_5 [Figs. 4(a), 4(b) and 5(a), 5(b), submitted to EPAPS][42] is consistent with this charge donation and back-donation scheme through orbital mixings.

IV. CONCLUSIONS

Large-scale CASMCSCF, MRSDCI, as well as DFT/B3LYP calculations have been carried out on the different electronic states of Nb_n and Nb_n^- ($n=4,5$). We have predicted the geometric and electronic properties of the low-lying electronic states of these clusters that assisted in interpreting the observed PES (Ref. 3) of Nb_n^-. The electronic states of the Nb_4 and Nb_4^- clusters have been studied for the tetragonal (both C_{2v} and D_{2h} type) and pyramidal (C_s) structures. The electronic states of the Nb_5 and Nb_5^- have been studied for the various geometrical arrangements. They include regular and distorted trigional bipyramid, regular and distorted tetragonal pyramid, and edge-capped tetrahedron. The studies have expounded on the Nb-Nb bonding characteristics and have revealed considerable involvement of both the 5*s* and 4*d* orbitals together with the 5*p* orbital of the Nb atom in the bond. The current study has not only aided understanding of the experimental findings on the PES (Ref. 3) of Nb_n^- ($n=4,5$), but also predicted properties such as EA, IP, and D_e of Nb_n ($n=4,5$), which compare very well with the available experimental[5,6,39] data. This gives confidence to our findings on the geometric and electronic properties of the different electronic states of Nb_n and Nb_n^- ($n=4,5$).

The CASMCSF/MRSDCI energy calculations and the analysis of the electronic configurations have shown that the ground ($^1A', C_s$) and the low-lying electronic states of Nb_4 exhibit $T\otimes e$ Jahn-Teller[23] distortion. Although our present DFT/B3LYP calculations and the earlier DFT calculations[17] agree on the energy ordering of the low-lying electronic

states of Nb_4, the Jahn-Teller effect of the ($^1A'$) electronic states of Nb_4 could not be explained through this method. The DFT/B3LYP method calculates the E state of the T_d structure as a higher root and thus fails to yield proper Jahn-Teller description of the electronic states. For the D_{2h} structure, of course, both the DFT/B3LYP and CASMCSCF/MRSDCI results agree on the $E\otimes b_1$ type Jahn-Teller distortion[23] of the B_{2u}, B_{3u}, B_{3g}, and B_{2g} states.

The ground state of the Nb_5 ($^2A_2$,DTB) cluster has been found to undergo $E\otimes e$ Jahn-Teller[23] distortion. Both the CASMCSCF/MRSDCI and DFT/B3LYP calculations support such a distortion. The only difference is that, while the DFT/B3LYP method predicts the energy separations of the two Jahn-Teller components, viz., $^2A_2$ and $^2B_1$, to be nearly degenerate ($\Delta E = 0.07$ eV), the CASMCSCF/MRSDCI predicts the energy separation of these two electronic states to be considerably higher ($\Delta E = 1.47$ eV). The CASMCSCF/MRSDCI method also predicts higher geometric distortion of the $^2B_1$ state. The present DFT/B3LYP and CASMCSCF/MRSDCI results are a bit different from the earlier DFT (Ref. 18) studies. The earlier DFT calculations predicted the ground state to be a doublet state with a trigonal bipyramid structure. Structural distortions were not predicted in the previous studies.

We have suggested tentative assignments of the observed PES (Ref. 3) of Nb_n^- ($n=4,5$) on the basis of our computed energy separations. Our CASMCSCF/MRSDCI results based on the $^1A'$ ground state (1.15 eV peak) of Nb_4 assign the first two strong peaks of the observed spectra at 1.6 and 2.0 eV as the ^1A_g and the $^3B_{3u}$ states. The $^5A'$ (C_s) and $^5B_{1g}$ (D_{2h}) states have been assigned for the peak at 2.9 eV. This peak is actually very broad (extending beyond 3.0 eV). Three different electronic states, viz., $^5A''$, $^3B_{1g}$, and $^5B_{3g}$ could be assigned to this peak. Two weak peaks of Nb_4^- at 2.5 and 3.4 eV were assigned tentatively to the $^1A''$, $^3B_{2u}$, $^1B_{1g}$, $^3A'$ (for 2.5 eV), $^1B_{1g}$, $^1B_{2u}$, and $^3A''$ (for 3.4 eV).

The PES (Ref. 3) of Nb_5^- has three peaks at 1.65, 2.4 (with a shoulder at 2.0 eV), and 3.2 eV. On the basis of the CASMCSCF/MRSDCI ground state of Nb_5 ($^2A_2$, DTB, 1.65 eV peak), the 2.0 eV shoulder peak has been assigned to the $^4A_1$ (DTB) and $^4B_1$ (DTB) states. The intense peak at 2.4 eV has been attributed to the $^4A_1$ (DTP), $^2A_1$ (DTB), and $^6B_2$ (DTB) states. According to the MRSDCI+Q energy separation, the $^2A''$ (DECT) state is also a possible candidate for this peak. The $^6B_1$ (DTP) state has been assigned as the probable candidate for the peak at 3.2 eV. Apart from these intense peaks, the PES of Nb_5^- has a shoulder peak at 2.9 eV and a weak peak at 3.4 eV. The electronic states $^6A_1$ (DTB), $^6A_2$ (DTP) have been assigned for the shoulder peak (2.9 eV), while the $^6A''$ (DECT), $^4B_2$ (DTP), and $^2B_2$ (DTP) states are potential candidates for the 3.4 eV peak.

The PES (Ref. 3) predict the vertical EA of Nb_4 and Nb_5 as 1.15 eV and 1.65 eV, respectively. The DFT/B3LYP and MRSDCI results predict the ground state of Nb_4^- as $^2A'$ (C_s) and $^2B_{3g}$, respectively. According to the CASMCSCF/MRSDCI calculations, the ground state of Nb_5^- has two competitive ground states ($^3B_1$ and $^1A_1$) for the DTB structure. The DFT/B3LYP level of calculation also suggests two competitive ground states ($^1A_1$, and $^3A_2$, DTB). Our calculated adiabatic EA values based on these ground states of Nb_4^- and Nb_5^- agree with the experimental results very well (Table X). The computed IP, D_e, and the AE of the Nb_4 and Nb_5 clusters are all in excellent agreement with the experiment.[5,6,39]

The orbital compositions, Mulliken populations, and the difference density plots further suggest that there is considerable electron donation and back donation in the formation of the Nb-Nb bonds in different electronic states. The involvement of the $5p$ orbitals of Nb in the Nb-Nb bonding indicates that there is considerable multiple-bond character and it imparts high stability to the Nb_4 and Nb_5 clusters. The calculated and the experimental D_e values of Nb_4 and Nb_5 are in agreement with this observation.

ACKNOWLEDGMENTS

This research was supported by the U.S. Department of Energy under Grant No. DEFG2-86ER13558. The work at LLNL was performed under the auspices of U.S. Department of Energy by the University of California under Contract No. W-7405-Eng.

[1] C. Berg, T. Schindler, G. Niedner-Schatteburg, and V. E. Bondybey, J. Chem. Phys. **102**, 4870 (1995).
[2] A. Berces, P. A. Hackett, L. Lian, S. A. Mitchell, and D. M. Rayner, J. Chem. Phys. **108**, 5476 (1998).
[3] H. Kietzmann, T. Morenzin, P. S. Bechthold, G. Gantefor, W. Eberhardt, D.-S. Yang, P. A. Hackett, R. Fournier, T. Pang, and C. Chen, Phys. Rev. Lett. **77**, 4528 (1996).
[4] A. B. Vakhtin and K. Sugawara, J. Chem. Phys. **111**, 10859 (1999).
[5] S. K. Loh, L. Lian, and P. B. Armentrout, J. Chem. Phys. **91**, 6148 (1989).
[6] D. A. Hales, L. Lian, and P. B. Armentrout, Int. J. Mass Spectrom. Ion Processes **102**, 269 (1990).
[7] V. E. Bondybey and J. H. English, J. Chem. Phys. **74**, 6978 (1981).
[8] T. G. Dietz, M. A. Duncan, D. E. Powers, and R. E. Smalley, J. Chem. Phys. **74**, 6511 (1981).
[9] M. E. Geusic, M. D. Morse, and R. E. Smalley, J. Chem. Phys. **82**, 590 (1985).
[10] M. D. Morse, M. E. Geusic, J. R. Heath, and R. E. Smalley, J. Chem. Phys. **83**, 2293 (1985).
[11] Y. M. Hamrick and M. D. Morse, J. Phys. Chem. **93**, 6444 (1989).
[12] P. P. Radi, G. von Helden, M. T. Hsu, P. R. Klemper, and M. T. Bowers, Int. J. Mass Spectrom. Ion Processes **109**, 49 (1991).
[13] D. B. Pederson, D. M. Rayner, B. Simard, M. A. Addicoat, M. A. Buntine, G. F. Metha, and A. Fielicke, J. Phys. Chem. A **108**, 964 (2004).
[14] M.-M. Rohmer and M. Benard, Chem. Rev. (Washington, D.C.) **100**, 495 (2000).
[15] S. Wei, B. C. Guo, H. T. Deng, K. Kerns, J. Purnell, S. A. Buzzu, and A. W. Castleman, Jr., J. Am. Chem. Soc. **116**, 4475 (1994).
[16] D. Dai, S. Roszak, and K. Balasubramanian, J. Phys. Chem. A **104**, 9760 (2000).
[17] J. E. Fowler, A. Garcia, and J. M. Ugalde, Phys. Rev. A **60**, 3058 (1999).
[18] L. Goodwin and D. R. Salahub, Phys. Rev. A **47**, R774 (1993).
[19] H. Gronbeck, A. Rosen, and W. Andreoni, Phys. Rev. A **58**, 4630 (1998); M. B. Knickelbein and S. Yang, J. Chem. Phys. **93**, 1476 (1990); **93**, 5760 (1990).
[20] R. Fournier, T. Pang, and C. Chen, Phys. Rev. A **57**, 3683 (1998).
[21] D. Majumdar and K. Balasubramanian, J. Chem. Phys. **119**, 12866 (2003).
[22] E. R. Davidson, J. Am. Chem. Soc. **99**, 397 (1977).
[23] I. B. Bersuker, Chem. Rev. (Washington, D.C.) **101**, 1067 (2001).
[24] I. B. Bersuker, *The Jahn-Teller Effect and Vibronic Interaction in Modern Chemistry* (Plenum, New York, 1984).
[25] F. Jensen, J. Chem. Phys. **102**, 6706 (1995).
[26] R. G. Parr and W. Wang, *Density Functional Theory of Atoms and Molecules* (Oxford University Press, New York, 1989).
[27] A. D. Becke, J. Chem. Phys. **98**, 5648 (1993).

[28] S. H. Vosko, L. Wilk, and M. Nusair, Can. J. Phys. **58**, 1200 (1980).
[29] C. Lee, W. Wang, and R. G. Parr, Phys. Rev. B **37**, 785 (1988).
[30] L. A. LaJohn, P. A. Christiansen, R. B. Ross, T. Atashroo, and W. C. Ermler, J. Chem. Phys. **87**, 2812 (1987).
[31] D. Majumdar and K. Balasubramanian, J. Chem. Phys. **115**, 885 (2001).
[32] S. R. Langhoff and E. R. Davidson, Int. J. Quantum Chem. **S9**, 183 (1975).
[33] M. J. Frisch, G. W. Trucks, H. B. Schlegel *et al.*, GAUSSIAN 98, Revision A.7 (Gaussian, Inc., Pittsburgh, PA, 1998).
[34] M. W. Schmidt *et al.*, J. Comput. Chem. **14**, 1347 (1993).
[35] The major authors of ALCHEMY II are B. Liu, B. Lengsfield, and M. Yoshimine.
[36] K. Balasubramanian, Chem. Phys. Lett. **127**, 324 (1986).
[37] M. Anderson, H. Gornbeck, L. Holmgren, and A. Rosen, in *Laser Techniques for the State Selected State to State Chemistry III*, edited by J. W. Hepburn (SPIE International Society for Optical Engineering, Bellingham, WA, 1995), Vol. 2548, p. 157.
[38] K. Balasubramanian and X. Zhu, J. Chem. Phys. **114**, 10375 (2001).
[39] M. B. Knickelbein and S. Yang, J. Chem. Phys. **93**, 5760 (1990).
[40] K. Balasubramanian, *Relativistic Effects in Chemistry Part A: Theory & Techniques* (Wiley-Interscience, New York, 1997), p. 301.
[41] K. Balasubramanian, *Relativistic Effects in Chemistry Part B: Applications to Molecules & Clusters* (Wiley-Interscience, New York, 1997), p. 527.
[42] See EPAPS Document No. E-JCPSA6-121-301430 for the difference density plots. A direct link to this document may be found in the online article's HTML reference section. The document may also be reached via the EPAPS homepage (http://www.aip.org/pubservs/epaps.html) or from ftp.aip.org in the directory /epaps/. See the EPAPS homepage for more information.